Lava flow eruption conditions in the Tharsis Volcanic Province on Mars

Sean Peters[1], Philip Russel Christensen[1], and Amanda B Clarke[1]

[1]Arizona State University

November 21, 2022

Abstract

Volcanism has played a major role in modifying the Martian surface. The Tharsis Volcanic Province dominates the western hemisphere of the planet with numerous effusive volcanic constructs and deposits. Here, we present the results of an in-depth study aimed at characterizing and modelling the emplacement conditions of 40 lava flows in the Tharsis Volcanic Province. These lava flows display a range of lengths (~15 – 314 km), widths (~0.5 – 29 m), and thicknesses (~11 – 91 km). The volumes and flow masses range from ~1 – 430 km3 and ~1011 – 1014 kg, respectively. Using three different models, we calculated a range of eruption rates (0.2 – 3.5 x 104 m3/s), viscosities (104 – 107 Pa s), yield strengths (800 – 104 Pa), and emplacement times (14 hours – 22 years). While the flow lengths and volumes are typically larger than terrestrial lava flows by an order of magnitude, rheologies and eruption rates are similar based on our findings. Emplacement times suggest that eruptions were active for long periods of time, which implies the presence and persistence of open subsurface pathways. Differences in flow morphology and emplacement conditions across localities within Tharsis highlight different pathways and volumes of available material between the central volcanoes and the plains. The scale of the eruptions suggests there could have been eruption-driven local, regional, and perhaps, global impacts on the Martian climate. The relatively recent age of the eruptions implies that Mars has retained the capability of producing significant localized volcanism.

1 **Title**

2 Lava flow eruption conditions in the Tharsis Volcanic Province on Mars

3

4 S. I. Peters[1], P. R. Christensen[1], and A.B. Clarke[1,2]. [1]School of Earth and Space Exploration,

5 Arizona State University, Tempe, AZ 85281, USA. [2] Istituto Nazionale di Geofisica e

6 Vulcanologia, Sezione di Pisa, Pisa, Italy.

7

8 Corresponding author: Sean I. Peters, School of Earth and Space Exploration, Arizona State

9 University, Tempe, AZ, 85281, USA. (speter24@asu.edu)

10

11 **Key Points:**

12 - Terrestrial effusion rates and compositions explain many Martian lava flow

13   morphologies

14 - Martian lava flows require large and/or long-lived subsurface pathways to transport

15   large volumes to surface

16 - Differences in eruption rates across Tharsis indicate different source conditions and

17   different conditions in subsurface conduits

18

19   **Abstract**

20   Volcanism has played a major role in modifying the Martian surface. The Tharsis

21   Volcanic Province dominates the western hemisphere of the planet with numerous effusive

22   volcanic constructs and deposits. Here, we present the results of an in-depth study aimed at

23   characterizing and modelling the emplacement conditions of 40 lava flows in the Tharsis

24   Volcanic Province. These lava flows display a range of lengths (~15 – 314 km), widths (~0.5 –

25   29 m), and thicknesses (~11 – 91 km). The volumes and flow masses range from ~1 – 430 km^3

26   and ~10^{11} – 10^{14} kg, respectively. Using three different models, we calculated a range of

27   eruption rates (0.2 – 3.5 x 10^4 m^3/s), viscosities (10^4 – 10^7 Pa s), yield strengths (800 – 10^4 Pa),

28   and emplacement times (14 hours – 22 years). While the flow lengths and volumes are typically

29   larger than terrestrial lava flows by an order of magnitude, rheologies and eruption rates are

30   similar based on our findings. Emplacement times suggest that eruptions were active for long

31   periods of time, which implies the presence and persistence of open subsurface pathways.

32   Differences in flow morphology and emplacement conditions across localities within Tharsis

33   highlight different pathways and volumes of available material between the central volcanoes

34   and the plains. The scale of the eruptions suggests there could have been eruption-driven local,

35   regional, and perhaps, global impacts on the Martian climate. The relatively recent age of the

36   eruptions implies that Mars has retained the capability of producing significant localized

37   volcanism.

38

39   **Plain Language Summary**

40   Volcanoes have resurfaced a majority of the Martian surface. Understanding the volcanic

41   history of Mars is critical to understanding the evolution of the planet. Lava flows are one of the

42   most common volcanic features on Mars, and numerous examples are present in the Tharsis

43 volcanic province on shield volcanoes and in vast volcanic plains. Using three different

44 approaches, we characterized the eruption conditions of 40 lava flows. In addition, we measured

45 their dimensions and calculated volumes and masses. We observed flow dimensions (e.g.

46 lengths and volumes) larger than typical terrestrial lava flows. Viscosities and yield strengths

47 were similar to terrestrial values; however, effusion rates were generally at the higher end of

48 terrestrial rates. These results indicate that lava flows erupted on Mars did not require exotic

49 compositions or exceptionally high eruption rates to be emplaced. However, this does imply

50 longer eruption times which requires the existence of long-lived subsurface conduits capable of

51 transporting magma to the surface.

52

1. Introduction

Volcanism is a fundamental geologic process that has created and shaped the surfaces of the terrestrial planets in our solar system [*Carr,* 1973; *Carr,* 1974; *Greeley and Spudis*, 1981; *Wilson and Head*, 1983; *Pieri et al.*,1984; *Gregg and Fink*, 2000; *Plescia*, 2004; *Werner*, 2009; *Spudis et al.*, 2013].   The volcanic history of a planetary body provides information on its formation and evolution [*Carr,* 1973; *Carr,* 1974; *Greeley and Spudis*, 1981; *Wilson and Head*, 1983; *Spudis et al.*, 2013].   For Mars, where ~60% of the crust has been resurfaced by effusive volcanism, a variety of volcanic landforms have been preserved at the surface, including vast lava flow plains, sinuous rilles, massive shield volcanoes, cinder cones, and ash shields [*Carr,* 1974; *Greeley and Spudis*, 1981; *Plescia*, 2004; *Werner*, 2009; *Hauber et al.,* 2011; *Hiesinger et al.,* 2009; *Xiao et al*., 2012].   The bulk of Martian volcanism appears to have occurred early in the planet's history (>3Ga), with decreasing volcanic fluxes through time [*Werner,* 2009; *Tanaka et al.*¸2014].   Despite an abundance of volcanic features on Mars, the volcanic history of the planet remains complicated due to the lack of global compositional data, the lack of human observation during volcanic activity, and sometimes a lack of analogous terrestrial terrain and processes.

Using flow morphology to estimate eruption conditions has been a goal of terrestrial and planetary volcanology for decades and has fueled a number of studies [e.g., *Wilson and Head,* 1983; *Fink and Griffiths,* 1990; *Gregg and Fink,* 1996; *Cashman et al.*, 1998; *Glaze and Baloga*, 2006; *Hiesinger et al.,* 2007; *Baloga and Glaze*, 2008; *Hauber et al.,* 2011].   In the absence of direct observations, the eruption conditions and flow properties can be estimated based upon the morphology of preserved deposits.   These deposits provide a snapshot into the planet's interior and composition.   Previous studies have estimated lava flow eruption rates, viscosities, yield

76 strengths, and emplacement times using combinations of simplified fluid mechanics, numerical

77 models, deposit morphology, and morphometry [e.g. *Griffiths and Fink*, 1992; *Gregg and Fink*,

78 1996; *Glaze and Baloga*, 2006; *Baloga and Glaze*, 2008; *Glaze et al.,* 2009; *Hauber et al.,* 2011;

79 *Hiesinger et al.,* 2009].

80   In this study, we have observed and quantified the morphology and dimensions of 40 lava

81 flows in the Tharsis Volcanic Province on Mars in order to calculate eruption rates, viscosities,

82 yield strengths, and emplacements times. These 40 lava flows occur in the volcanic plains and in

83 proximity to or on central volcanoes. High resolution images up to 0.4 m/pixel and digital

84 terrain models at ~50 – 70 m/ pixel have enabled detailed analyses of these lava flows [*Jaumann*

85 et al., 2007; *Malin* et al., 2007; *McEwan* et al., 2007]. We have applied three lava flow

86 emplacement models that utilize flow morphology and morphometry to constrain eruption rates,

87 rheology, and emplacement times, and compared those results to a wide range of analogous

88 terrestrial data. The suite of models consists of 1) a standard cooling-limited rheologic treatment

89 outlined in *Hiesinger et al.* [2007]; 2) the utilization of the non-dimensional parameter Ψ derived

90 from laboratory analogue experiments; and 3) the self-replication model outlined in *Baloga and*

91 *Glaze* [2008]. The calculated volumes, eruption rates, viscosities, and emplacement times are

92 interpreted in terms of their implications for the eruption conditions of relatively recent volcanic

93 activity on Mars and the subsurface pathways that transport magma in the Martian crust. An

94 application of this method to lava flows on other volcanic bodies, such as Io or Venus, could also

95 prove useful.

96 **2. Background**

97   The eruption conditions of lava flows on Mars have implications for understanding its

98 composition, interior, and evolution. The morphology of terrestrial and extraterrestrial lava
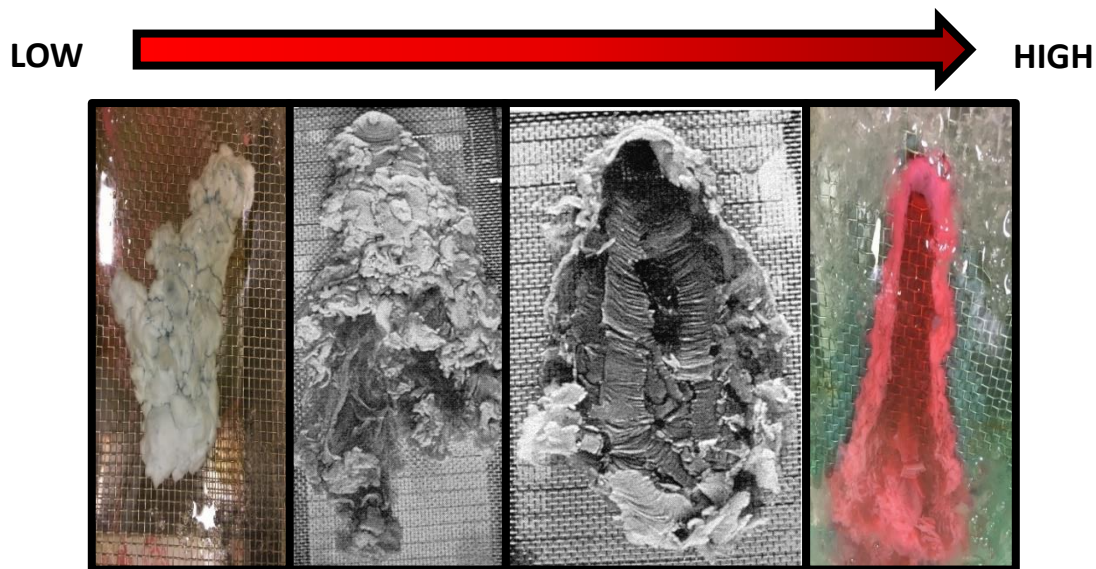
flows has long been used as a proxy for the eruptive conditions at the time of emplacement [e.g., Walker 1971, 1973; *Carr*, 1973, 1974; *Wilson and Head*, 1983; *Griffiths and Fink*, 1992; *Gregg and Fink*, 1996; *Cashman et al.*, 1998; *Bleacher et al.*, 2007; *Hiesinger et al.*, 2007; *Baloga and Glaze*, 2008; *Hauber et al.*, 2011]. A number of studies have used the morphology and morphometry of lava flows on Mars to estimate effusion rates, viscosities, and yield strengths by applying cooling limited and rheologic models [*Wilson and Head*, 1983; *Glaze and Baloga*, 2006; *Bleacher et al.*, 2007; *Hiesinger et al.*, 2007; *Hauber et al.*, 2011]. These studies have necessarily made a variety of simplifying assumptions about lava flow rheology, composition, and environmental conditions during emplacement. Some studies have invoked either exceptional eruption rates never observed in terrestrial lava flows or exotic compositions to explain the very large dimensions of Mars lava flows [e.g., *Wilson and Head*, 1983; *Cashman et al.*, 1998 and references therein; *Garry et al*., 2007; *Giacomini et al.,* 2009]. These analyses were partly predicated on the following assumptions: the length of lava flows is controlled exclusively or largely by eruption rate; the entire flow front is active at all times with the flow moving as a coherent mass; and/or lava behaves as a Newtonian fluid [*Nichols*, 1939*; Bruno et al.*, 1996; *Baloga et al.*, 1998; *Baloga and Glaze,* 2008]. Although studies have demonstrated a Newtonian rheology may be assumed for the hot interior of a lava flow, *Hulme* [1976] demonstrated that the behavior of lava flows on Olympus Mons, Mars, and elsewhere, were better approximated by a Bingham rheology due to the significant yield strength of most lavas, particularly as they propagate and cool. Subsequent studies followed suit [e.g. *Bruno et al.*, 1996; *Hiesinger et al.,* 2007; *Glaze and Baloga*, 2006; *Baloga and Glaze,* 2008; *Hauber et al.*, 2011]. Recent works have accounted for more complex processes that occur during the emplacement of lava flows such as levee construction and overspills [*Baloga et al.*, 1998; *Baloga*

122 *and Glaze*, 2008; *Glaze et al.*, 2009]. Most studies aimed at constraining lava composition and

123 effusion rates on Mars have focused on the Tharsis and Elysium volcanic provinces where some

124 of the best-preserved lava flows on the planet are located. Due to dust cover, however,

125 compositional data is sparse to nonexistent in these localities [*Christensen*, 1986; *Hiesinger et*

126 *al.,* 2007; *Baloga and Glaze,* 2008; *Hauber et al.*, 2011; *Rogers and Christensen,* 2007].

127 However, a basaltic to basaltic andesite composition of much of the Martian crust has been

128 determined using thermal infrared spectral measurements of less dust covered regions [*Rogers*

129 *and Christensen*, 2007]. Based on the moderate range of compositions observed in the dust-free

130 regions, it is likely that the Tharsis region is basaltic as well.

131   Laboratory analogue experiments have provided a fundamental understanding of lava

132 flow emplacement processes and their relationship to propagation rate and morphology, and have

133 thus been used to make predictions of lava flow behavior on other planets [*Fink and Griffiths,*

134 1990; *Griffiths and Fink,* 1992; *Gregg and Fink,* 1996; 2000; *Blake and Bruno,* 2000; *Soule and*

135 *Cashman,* 2004; *Rader et al.,* 2017; *Peters*, 2020]. Previous laboratory studies have examined

136 lava flow morphologies by extruding substances analogous to lava into controlled environments

137 under controlled source conditions [*Fink and Griffiths,* 1990, 1992; *Gregg and Fink,* 1996,

138 2000]. Polyethylene glycol (PEG) wax has been demonstrated to be a useful analogue to real

139 lava flows due to its temperature dependent viscosity and timescale of surface crust formation

140 [*Fink and Griffiths,* 1990, 1992; *Gregg and Fink,* 1996, 2000; *Soule and Cashman*, 2004]. *Fink*

141 *and Griffiths* [1990] derived a dimensionless parameter, Ψ, which is a ratio of the characteristic

142 time scale of crust formation, which is controlled by surface cooling, to the characteristic time

143 scale of lateral thermal advection, for which flow propagation rate is a proxy.

144   *Fink and Griffiths* [1990] observed five morphologies produced in the laboratory: no

145   crust, levees, folds, rifts, and pillows, which occur on a continuum from high to low Ψ values,

146   respectively (Fig. 1). Analogous morphologies have been observed in nature [*Fink and Griffiths,*

147   1990, 1992; *Griffiths and Fink,* 1992; *Gregg and Fink,* 1996]. Subsequent studies utilized PEG

148   experiments to address slope effects [e.g., *Gregg and Fink*, 2000]. Extrapolating laboratory

149   experiments to other terrestrial bodies such as Mars has been attempted in order to constrain

150   eruption parameters and predict expected morphologies, although the image resolution at the

151   time of these studies was limited to >150 m/pixel [*Fink and Griffiths*, 1992; *Gregg and Fink,*

152   1996; *Peters*, 2020]. Laboratory experiments, in conjunction with rheologic modelling and

153   remote sensing geomorphology, therefore provide an additional constraint on prehistoric
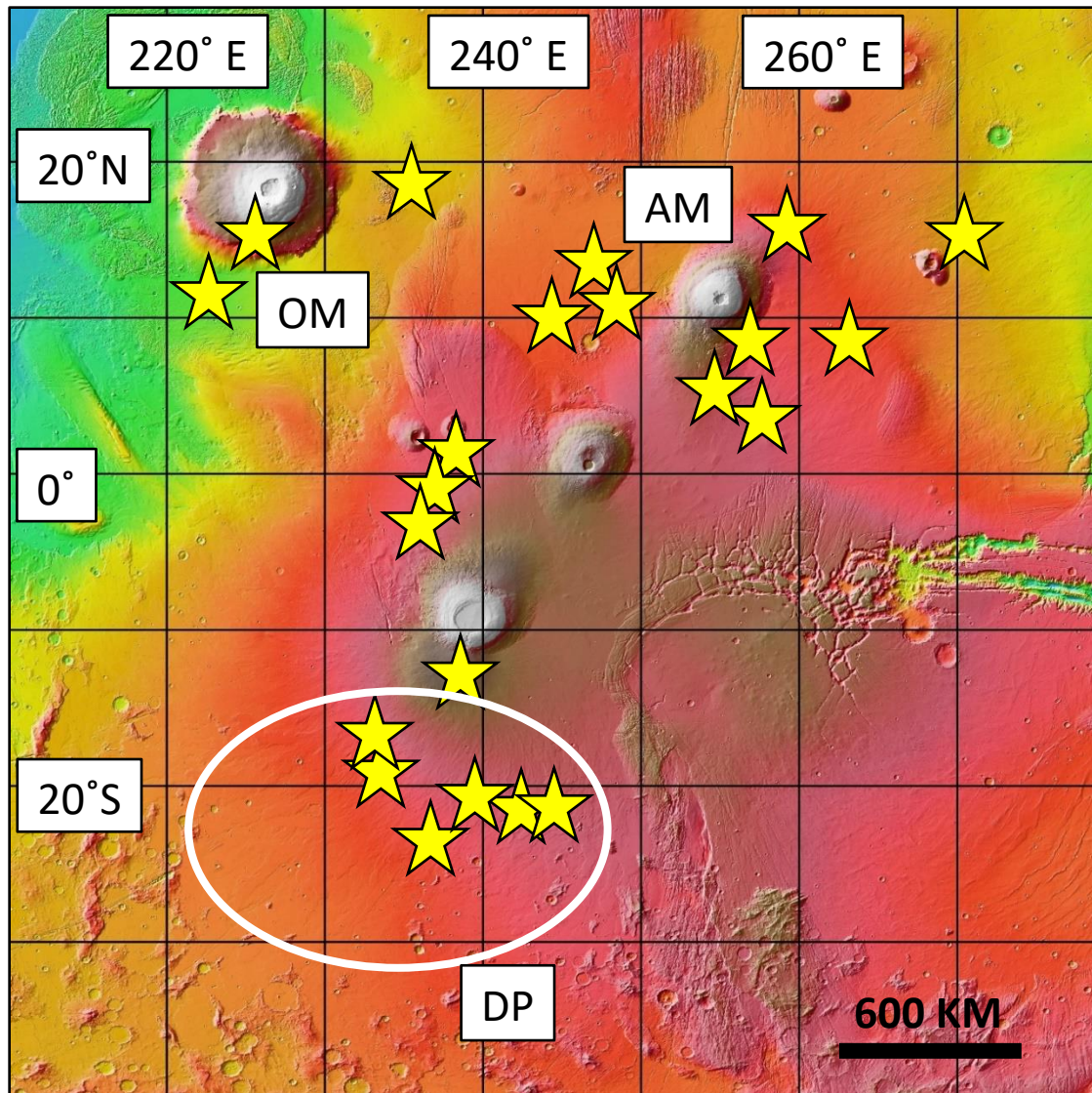
154   eruption conditions on Mars.

156   **Figure 1:** Examples of the four primary morphologies observed by *Fink and Griffiths* [1990],
157   *Gregg and Fink* [2000], and *Peters* [2020]. From low to high Ψ, the morphologies are Pillows,
158   Rifts, Folds, and Levees. Modified from Gregg and Fink, 2000.

161   **3.** Geologic Setting

162   3.1. Tharsis Volcanic Province

163   The Tharsis region represents the largest volcanic province on Mars (Fig. 2), containing

164   the tallest volcano in the solar system (Olympus Mons at ~22 km), one of the largest volcanoes

165   on the planet in areal extent (Alba Mons at ~1.15 x 10^6 km^2), and the Tharsis Montes – three

166   large shield volcanoes [*Carr,* 1973; *Carr,* 1974; *Crumpler and Aubele*, 1978; *Greeley and*

167   *Spudis*, 1981; *Scott and Tanaka*, 1981; *Plescia*, 2004].   In addition, the region contains

168   innumerable lava flows and small shields, in what is sometimes characterized as plains-style

169   volcanism [*Greeley,* 1977; *Baloga and Glaze,* 2008; *Glaze et al.,* 2009; *Hiesinger et al.,* 2007;

170   *Hauber et al.,* 2011].   Tharsis dominates the western hemisphere of the planet and occupies a

171   region from ~60° N to ~40° S and 210° E to 300° E and ~4000 x 6000 km.   Volcanic activity

172   began ~4 Ga and has occurred within the last ~100 Ma [*Carr,* 1973; *Carr,* 1974; *Scott and*

173   *Tanaka*, 1981; *Plescia*, 2004; *Werner,* 2009].   The 40 lava flows featured in this study occur

174   throughout the Tharsis Volcanic Province, primarily on and around Olympus Mons, in the

175   volcanic plains surrounding the Tharsis Montes, and Daedalia Planum.   A brief summary is

176   given of each region.

Figure 2: Map of study area, the Tharsis Volcanic Province. Base map is MOLA colorized topography, with warm colors representing areas of higher elevation. Square label demarks Olympus Mons (OM) and Ascraeus Mons (AM), while white circle encompasses Daedalia Planum (DP).

3.1.1. Olympus Mons & Ascraues Mons

Olympus Mons and Ascraues Mons are two large shield volcanoes in the Tharsis volcanic province. Olympus Mons is 600 km across and 22 km high and Ascraues Mons is 400 km across and 15 km high. Olympus Mons and is situated northwest of the Tharsis Montes and southwest of Alba Mons (Fig. 2), while Ascraeus Mons (located east of Olympus Mons) is the

188 northernmost of the Tharsis Montes [*Carr*, 1973; *Greeley and Spudis*, 1981; *Plescia*, 2004;

189 *Werner*, 2009]. Both volcanoes display nested caldera complexes and evidence of widespread

190 effusive eruptions. Extensive dust cover prohibits compositional analyses of either volcano, but

191 both volcanoes are morphologically similar to Hawai'i and the Galapagos shield volcanoes and a

192 basaltic composition has been inferred for their erupted lavas [e.g., *Christensen*, 1986; *Bleacher*

193 et al., 2007; *Byrne et al.*, 2012; *Rogers and Christensen*, 2007]. Both volcanoes display gentle

194 sloping flanks (~4 – 6˚) with some steepening on the upper flanks [e.g., *Plescia*, 2004].

195 Although construction of Olympus Mons and Ascraeus Mons is believed to have been largely

196 completed by the Late Noachian or Early Hesperian (>3.6 Ga), their surfaces have been dated to

197 ~100 – 800 Ma based on crater count modeling [e.g. *Neukum* et al., 2004; *Werner*, 2009; *Xiao et*

198 *al.*, 2012]. Some of the youngest features on Olympus Mons and Ascraeus Mons include lavas

199 on the floors of the nested calderas (~100–200 Ma), some flank lava flows (~50 Ma), and small

200 satellite vents and arcuate graben [e.g., *Neukum* et al., 2004; *Werner*, 2009; *Byrne et al.*, 2012;

201 *Tanaka et al.*, 2014; *Peters and Christensen,* 2017].

202 3.1.2. Volcanic plains & Daedalia Planum

203   Volcanic plains formed by countless overlapping lava flows cover much of the terrain

204 within the Tharsis Volcanic Province (Fig. 2) producing a monotonous topography of gentle

205 slopes, punctuated by low shields, cinder cones, graben, and the central volcanoes [e.g., *Carr,*

206 1973, 1974; *Greeley and Spudis*, 1981; *Hauber et al.,* 2011]. Individual lava flows can extend

207 hundreds of kilometers from their sources, which include dozens of low shield volcanoes, the

208 Tharsis Montes, and buried sources [*Carr,* 1973, 1974; *Crumpler and Aubele*, 1978; *Greeley and*

209 *Spudis*, 1981; *Hiesinger et al.,* 2007; *Baloga and Glaze*, 2008; *Glaze et al.,* 2009; *Hauber et al.*,

210 2011]. Daedalia Planum – an example of this terrain – is an 18 x 10^6 km^2 volcanic plain on Mars

211 located southwest of Arsia Mons, one of the Tharsis Montes [*Plescia,* 2004; *Werner*, 2009;

212 *Giacomini et al.,* 2012]. It too hosts very long lava flows (>200 km in some cases), with many

213 believed to be sourced by activity related to Arsia Mons, the southernmost and oldest of the

214 Tharsis Montes [e.g., *Scott and Tanaka,* 1981; *Plescia,* 2004; *Giacomini et al.,* 2009, 2012;

215 *Werner*, 2009; *Crown and Ramsey*, 2016]. Recent studies on Daedalia Planum have measured

216 average lava flow thicknesses of 35 – 70 m using high resolution image and elevation data,

217 observed inflation in lava flows using possible lava rises and tumuli, and attempted

218 compositional analysis via spectral mapping [e.g., *Giacomini et al.,* 2009, 2012].

219 **4. Methodology**

220 4.1. Datasets & Analyses Criteria

221 We used image data from the Mars Reconnaissance Orbiter (MRO) Context Camera

222 (CTX: ~5 m/pixel), [*Malin* et al., 2007], the Mars Odyssey Thermal Emission Imaging System in

223 the infrared (THEMIS IR: 100 m/pixel), [*Christensen* et al., 2004], and the MRO High

224 Resolution Imaging Science Experiment (HiRISE: ~0.5 m/pixel) instruments [*McEwan* et al.,

225 2007]. We utilized topographic data from the Mars Global Surveyor (MGS) Mars Orbital Laser

226 Altimeter (MOLA: ~463 m/pixel) digital elevation model (DEM) [*Zuber* et al., 1992] dataset, as

227 well as Mars Express High-Resolution Stereo Camera (HRSC) DEM (DEM cell size: 50 – 75

228 m) [*Jaumann* et al., 2007]. While the Tharsis region has extensive CTX and localized HiRISE

229 coverage, high resolution HRSC DEMs did not cover the entire study area. As a result, some

230 flows were characterized using the MOLA DEM [e.g., *Glaze et al*., 2003]. Due to the resolution

231 of the MOLA DEM, larger lava flows were given priority when HRSC DEM coverage was not

232 available. All datasets were accessed and analyzed using the Java Mission Planning and Remote

233 Sensing (JMARS) GIS software [e.g., *Gorelick et al.,* 2003].

234   For this study, we considered lava flows in the Tharsis Volcanic Province because of the

235   large number of well-preserved flows and extensive overlapping datasets. We selected 40 lava

236   flows based on the following criteria: 1) morphology and 2) data coverage. We prioritized

237   flows with relatively unobstructed flow along their lengths and relatively well-defined margins.

238   In all cases, the full extent of the original flow was not preserved due to superimposed lava

239   flows, impact craters, or erosion/degradation. These processes reduced the available flow area

240   for study and also resulted in the erasure of the flow source. As a result, our flow lengths,

241   volumes, and volumetric flow rates represent minima. We also prioritized lava flows with

242   adequate data coverage. Every selected lava flow had CTX visible image coverage and at least

243   partial HRSC and/or MOLA DEM coverage. Despite the ~1 m dust mantle that blankets the

244   Tharsis Volcanic Province, lava flow surface texture is relatively well preserved and discernible

245   [*Christensen*, 1986]. Compression ridges are visible on a number of lava flows, owing to the

246   resilience of these features in the face of erosion, degradation, and dust cover. However, finer

247   scale morphologies, such as pahoehoe lava lobes (which tend to be meter-scale features), if

248   originally present, are not visible due to limited spatial resolution. Overall, the morphologies

249   and morphometric properties of lava flows in the Tharsis Volcanic Province suggest a basalt to

250   basaltic andesite composition [e,g., *Carr*, 1974; *Hulme*, 1974; *Bleacher et al.*, 2007; *Hiesinger et*

251   *al.*, 2007]. We measured and calculated the length, mean width, mean thickness, surface area,

252   volume, and mean slope for each of the 40 lava flows in this study (Table 1). The length of each

253   flow was measured using a centerline. The mean width and thickness of each flow were

254   calculated using multiple cross-sectional profiles. We calculated the volume by multiplying

255   surface area by mean thickness. We applied the three models discussed above to the 40 lava

256   flows in this study in order to estimate volumetric flow rates, bulk viscosities and yield strengths,

257 and emplacement times. The models and how they were applied to the data set are detailed in

258 the following section.

	Lat (N)	Long (E)	Region	Length (km)	Mean Width (km)	Flow Thickness (m)	Volume (km³)	Observed Ψ Morphology
Flow 1	18.53	235.94	E of Olympus Mons	21	5.61	10.5	1.32	Levee (fed by)
Flow 2	11.914	244.629	Tharsis	313	18.3	46	281.80	Levees
Flow 3	14.504	248.246	Tharsis	314	28.8	39	436.18	Smooth-Levees
Flow 4	15.199	226.654	Olympus Mons	18.3	0.592	27	0.38	Levee-Folds
Flow 5	15.008	226.823	Olympus Mons	33	0.57	11.5	0.25	Levee-Folds
Flow 6	15.761	224.764	Olympus Mons	19	3	25	1.48	Levees
Flow 7	11.739	224.015	S Olympus Mons	100	6.9	26	23.40	Levees
Flow 8	11.597	222.495	S Olympus Mons	41	6.5	14	1.76	Levees
Flow 9	-19.332	243.262	Daedalia Planum	78	5.9	25	12.00	Levee
Flow 10	-20.945	240.957	Daedalia Planum	136.5	5.89	33	34.16	Levee
Flow 11	-21.733	242.555	Daedalia Planum	58	16.3	35.5	38.41	Levee-Folds
Flow 12	-23.297	242.812	Daedalia Planum	266	19.3	45	268.16	Levees
Flow 13	-22.547	244.16	Daedalia Planum	201	11.8	30	101.07	Levees
Flow 14	-23.195	237.617	Daedalia Planum	219	6	32	52.22	Levee
Flow 15	-19.081	234.684	Daedalia Planum	92	3.8	15	6.11	Levee-Folds
Flow 16	-17.307	233.48	Daedalia Planum	164.5	3.23	16	12.24	Levees
Flow 17	-22.665	237.6084	Daedalia Planum	106	4.48	17	10.17	Levees
Flow 18	8.945	257.408	Ascraeus Mons	16	4.1	15	0.99	Folds
Flow 19	15.521	261.191	Ascraeus Mons	78.5	4.19	23	8.33	Levees
Flow 20	12.102	250.046	W of Ascraues Mons	99	12	37	65.38	Levees
Flow 21	11.193	248.41	W of Ascraues Mons	121	16.5	38	73.07	Smooth-Levees
Flow 22	15.757	225.213	Olympus Mons	15	1.15	17.5	0.33	Levees
Flow 23	15.814	225.379	Olympus Mons	30.4	5.93	91	8.20	Rifts
Flow 24	15.156	225.105	Olympus Mons	27.12	1.32	18	0.77	Levee
Flow 25	14.997	225.298	Olympus Mons	59.5	6.79	68	13.74	Rifts

Flow 26	16.089	227.269	Olympus Mons	13.3	3.72	64	1.58	Rifts
Flow 27	15.91	227.239	Olympus Mons	27.6	2.2	37	1.12	Rifts
Flow 28	15.178	259.464	Ascraeus Mons	47.6	4.6	30.8	3.37	Rifts
Flow 29	15.689	259.131	Ascraeus Mons	29	7	38.4	3.90	Rifts
Flow 30	8.572	263.609	Tharsis	43.7	7.13	29	8.96	Levee
Flow 31	-12.934	239.423	Daedalia Planum	25.3	2.08	31	1.72	Levee
Flow 32	-0.879	237.326	Tharsis	77.2	5.94	30.5	15.16	Levee
Flow 33	-3.006	239.936	Tharsis	69.3	6	29	11.66	Levee
Flow 34	16.210	261.309	Tharsis	72	3.67	25	7.13	Levee
Flow 35	5.018	256.914	Tharsis	98.6	3.11	16	5.09	Levee
Flow 36	5.229	254.687	Tharsis	23	1.26	11	0.46	Levee
Flow 37	5.371	255.546	Tharsis	38.4	1.86	13	1.09	Levee
Flow 38	3.576	259.678	Tharsis	128	4.94	18.1	11.91	Levee
Flow 39	1.347	238.558	Tharsis	71.1	6.7	23	12.03	Levee
Flow 40	15.51	271.857	Tharsis	219	13.8	55	173.69	Levee

259   **Table 1:** Data on 40 lava flows in Tharsis volcanic province on Mars investigated in this study.

260   4.2. Models for interpreting the datasets

261   4.2.1. *Cooling-limited and Rheologic Model*

262   We applied a standard rheologic treatment to 34 of 40 lava flows using methods outlined

263   by *Hiesinger et al.* [2007], and references therein, to calculate eruption rate and viscosity. Six of

264   40 lava flows were excluded because they exhibit prominent ridges likely formed through

265   repeated overspills from a channel or tube during emplacement, in stark contrast to the typical

266   flows for which this method was intended [*Sakimoto et al.*, 1997]. The method uses 1) the

267   Graetz number (G_z), a dimensionless number that characterizes the ratio of the time scale of

268   cooling by conduction at the edges or surface of the flow, to that of fluid advection downstream;

269   and 2) Jefferey's equation, which is a steady-state momentum equation reduced to a force

270   balance between downslope gravitational forces that drive the flow and viscous forces that

271   impede the flow, can be expressed in terms of flow velocity, geometry, and fluid viscosity

272   [*Jeffreys*, 1925; *Wilson and Head*, 1983]. This approach requires some assumptions including:

273   laminar flow of a Newtonian fluid; steady-state emplacement at low velocities; flow dimensions

274   that reflect rheological properties of the flow [e.g., *Wilson and Head,* 1983; *Hiesinger et al.*,

275   2007; *Hauber et al.*, 2011]; and a Graetz number of ~300 that defines when the flow halts,

276   following *Pinkerton and Sparks* [1976].

277   According to a suite of observations of cooling-limited lava flows at Mt. Etna, *Pinkerton

278   and Sparks* [1976] found that flows ceased advancing at G_z of approximately 300, when crust

279   extent and strength was sufficient to prevent the continued propagation of the small amount of

280   melt remaining in the core of the flows. *Gues*t et al. [1987] questioned the value of 300 because

281   *Pinkerton and Sparks* [1976] did not take into account branching of lava flows or the possibility

282   of volume-limited flows. However, for cooling-limited flows, Guest et al. [1987] place the

283 halting Graetz number at approximately 230, very close to the assumed value of 300. The Mars

284 flows studied here exhibit limited to no branching, and given their large volumes (see below),

285 they were unlikely to have been volume-limited. We therefore assume that they were cooling-

286 limited and proceed with a halting Graetz number value of 300. Graetz number (G_z) can be

287 expressed as

288

289 $$G_z = [Q/(\kappa x)]\,(w/h) \qquad \text{(Eq. 1)}$$

290

291 where Q is the effusion rate, κ is thermal diffusivity of the lava which is a function of its

292 composition ($m^2\ s^{-1}$), x is flow length, w is mean flow width (Table 1), and h is mean flow

293 thickness (Table 1) [*Wilson and Head,* 1983]. This equation is a modification of the original

294 Graetz number for cooling of a fluid in a cylindrical pipe. Eq. 1 accounts for the fact that thinner

295 flows cool faster than deeper flows by including the aspect ratio w/h [*Hulme and Fielder*, 1977].

296 Here effusion rate, Q, was obtained by rearranging Eq. 1, assuming a halting Graetz number of

297 300, using the flow geometries measured from the previously described data sets (Table 1), and

298 applying the thermal diffusivity of basalt, $5.00 \times 10^{-7}\ m^2/s$ [e.g., *Wilson and Head,* 1983; *Hon et*

299 *al.,* 1994; *Pasckert et al.*, 2012].

300 Jeffrey's equation can be used to relate the effusion rate of a flow to its viscosity, density,

301 and flow dimensions. It is derived for flow on an infinitely wide plane and is written as follows

302 for broad flows [*Jeffreys*, 1925].

303

304 $$\eta = \rho g h^3 w \sin\alpha\,/3Q \qquad \text{(Eq. 2)}$$

305

306   where η is the effective dynamic viscosity of the flow during emplacement and propagation, ρ

307   is the lava density during emplacement, *w* and *h* are the flow dimensions as described previously,

308   Q is volumetric effusion rate, α is the underlying slope, and 3 is a constant used for flows that are

309   much wider than they are deep [*Jeffreys*, 1925]. We assumed a density of 2700 kg/m^3 which is

310   consistent with estimates from previous studies and within the range of terrestrial basalt values

311   [e.g., *Rowland et al.*, 2004; *Hiesinger et al.*, 2007; *Hauber et al.*, 2011; *Pasckert et al.*, 2012]. Q

312   from Eq. 1, along with flow geometry, underlying slope, and magma density were used in Eq. 2

313   to calculate dynamic viscosity η. Emplacement times were estimated from Q and measured

314   individual flow volumes.

315   4.2.2.   *Laboratory experiments and Ψ*

316   We classified each of the 40 observed lava flows by dominant surface morphology,

317   which corresponds to a particular Ψ regime [*Fink and Griffiths,* 1990; *Gregg and Fink,* 1996]. Ψ

318   is a powerful way of understanding the dynamics of flow emplacement using only flow

319   morphology.   Because it is a dimensionless parameter, Ψ can be applied to flows of any

320   composition, rheology, and scale so long as reasonable emplacement constraints such as ambient

321   conditions and properties of the flowing liquid can be assumed.   Five flow morphologies

322   corresponding to discreet Ψ ranges have been observed. Those morphologies from high to low,

323    $\Psi > 55$ to $\Psi \sim 1$, are: No Crust, Levees, Folds, Rifts, and Pillows (Fig. 1) [*Fink and Griffiths,*

324   1990, 1992; *Gregg and Fink,* 2000]. Transitional morphologies are also observed in the lab and

325   on Mars, demonstrating that the morphologies are produced on a continuum. And, as stated

326   previously, the textures observed in the laboratory are observed in nature – from terrestrial felsic

327   lava flows to sulfur flows [e.g., *Fink et al.*, 1983; *Pieri et al.*, 1984; *Griffiths and Fink*, 1992;

328   *Gregg and Fink*, 1996; *Peters*, 2020].

329   In the analysis presented, we assumed that the predominant morphology observed

330   represents the dominant Ψ regime during the time of emplacement (Fig. 1). The validity of this

331   assumption has been demonstrated in the laboratory to the extent possible [*Fink and Griffiths,*

332   1990, 1992; *Gregg and Fink,* 2000]. Although there exists the possibility that flows pass through

333   a number of morphological regimes throughout the emplacement process, the final morphology

334   preserved in the rock record is the only source of data we have for the surface of Mars. We

335   proceed with this caveat in mind, and thus assume that our calculations based on Ψ regime best

336   represent the dominant flow emplacement conditions. Furthermore, each flow was assigned a Ψ

337   value range corresponding to the observed morphology. Some transitional morphologies (i.e.

338   levee-fold) were observed, while no pillow morphologies were definitively observed. We

339   interpreted the lava ridges, previously observed on Olympus Mons, Alba Mons, and other

340   localities, and interpreted as lava tubes [*Sakimoto et al.,* 1997; *Bleacher et al., 2007*], to represent

341   rift morphology. Our interpretation is based on laboratory analogue experiments using PEG wax

342   performed on slopes, which yielded ridge-like structures produced by lava tubes [*Peters*, 2020].

343   Ψ can be written in terms of a modified Peclet number, Π, a non-dimensional cooling

344   timescale for the crust, τ_s, and a ratio of temperature differences including ambient,

345   solidification, and wax or lava temperatures, θ_s [*Fink and Griffiths*, 1990, Eq. 10].

346

347                            $$\Psi = \Pi \tau_s(\theta_s) \quad \text{(Eq. 3)}$$

348

349   Π incorporates the traditional Peclet number (Pe), which is the ratio of the rate of

350   advective heat transport by the flowing lava to the rate of conductive heat transport at the flows

351   surface. Π also includes the effects of reduced gravity (g'), kinematic viscosity (ν), thermal

352 diffusivity of the wax or lava (κ), and the timescale (λ) over which the contact temperature of the

353 wax or lava reaches the temperature of the ambient environment far from the lava surface, where

354 the contact temperature is defined as the temperature at the interface between wax or lava and the

355 ambient.

356

357
$$\Pi = \left(\frac{g'}{\nu}\right)^{\frac{2}{3}} \kappa^{\frac{1}{3}} \lambda P e^{\frac{1}{3}} \quad \text{(Eq. 4)}$$

358

359 Like Pe, Π represents a ratio of a characteristic advective flux or flow rate downstream to

360 a characteristic thermal diffusion rate at the surface of the flow [*Fink and Griffiths*, 1990, Eq.

361 11].

362 Ψ can also be written as a ratio of the solidification and advection time scales, which is

363 more descriptive.

364

365
$$\Psi = \frac{t_s}{t_a} \quad \text{(Eq. 5)}$$

366

367 Here, t_s represents the timescale of solidification of the surface crust and t_a represents the

368 timescale of horizontal advection. Using the relationships in Eq. 3 and 4, we can calculate a

369 range of effusion rates corresponding to the Ψ ranges for each flow morphology, for assumed

370 Mars eruption and ambient conditions. From those effusion rates and measured flow volumes,

371 we can also calculate a range of emplacement times for each flow.

372 However, in order to translate the Ψ ranges to eruption rates, we are required to make

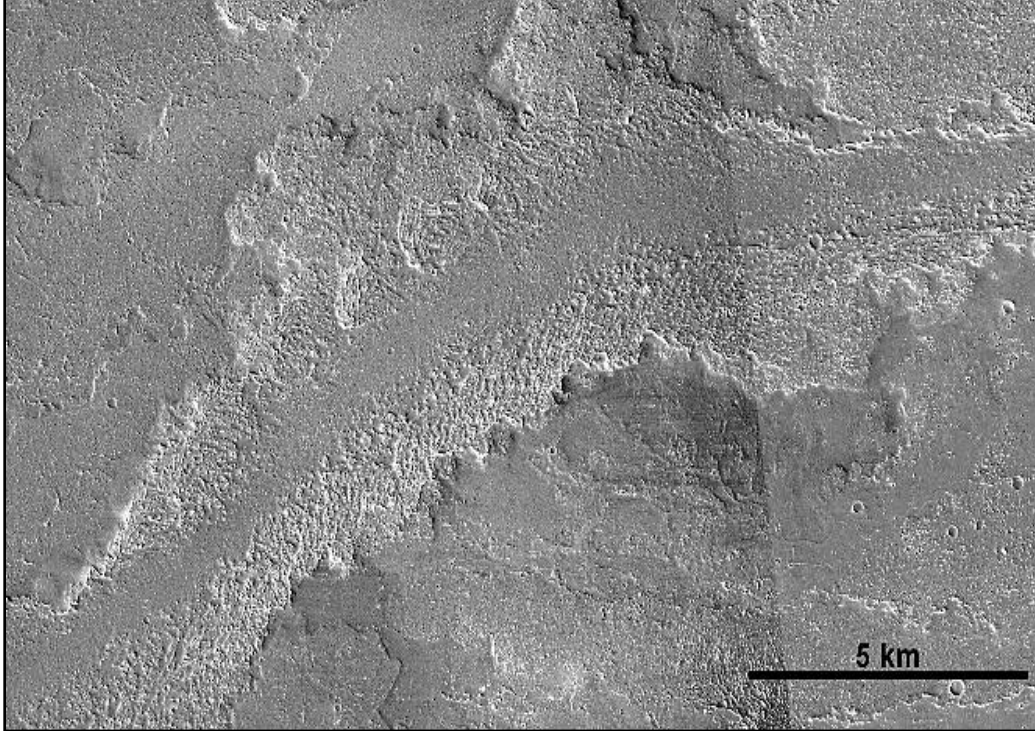373 simplifying assumptions about the ambient environment and the erupted liquid. In the lab, the

374 ambient environment corresponds to the chilled bath or a sucrose solution and the erupted fluid

375 refers to the PEG wax. For Mars, these values correspond to the ambient environment of the

376 Martian surface and the lava flow. We assumed that radiation is the primary way a lava flow

377 loses heat on Mars based on previous work, which found that radiant heat loss is an order of

378 magnitude greater than that for convection or conduction [e.g., *Griffiths and Fink,* 1992; *Gregg*

379 *and Fink,* 1996; *Rowland et al.*, 2004]. As a result, convective and conductive losses are

380 considered to be negligible. In addition to the flow properties mentioned previously (i.e. density,

381 thermal diffusivity), we assumed an ambient environment temperature of 210 K, an atmospheric

382 density of 0.02 kg/m^3, a solidification temperature of 900˚C, and gravity of 3.71 m^3/s [e.g., *Peck*,

383 1978; *Rowland et al.*, 2004]. The ambient environment temperature, atmospheric density, and

384 gravity represent the average values for Mars [e.g., *Rowland et al.*, 2004] and deviations of these

385 values do not significantly impact our results. For values related to the Martian atmosphere,

386 specifically kinematic viscosity, we assumed pure CO_2 [*Chemical Rubber Company*, 1984;

387 *Crane Company*, 1988]. The basalt solidus is cited as 980˚C; however, the internal temperature

388 of barely mobile basalt flows has been measured at temperatures as low as 800˚C and basalt

389 flows on Mt Etna have been typically modeled with solidification temperatures of ~870 ˚C

390 [*Peck*, 1978; *Pinkerton et al.*, 2002; *Vicari et al.*, 2007; *Belousov et al.*, 2015]. We find a value

391 of 900˚ C to be reasonable and within the range of previous studies. The solidification

392 temperature has the largest impact on Ψ effusion rate estimates, with a deviation of $\pm$ 50˚ C

393 yielding an order of magnitude difference. Lava density (2700 kg/m^3) had a similar impact, but

394 only if changed by >25%. We assumed the lava flows in our study erupted at 1150˚C, which is

395 similar to the erupted temperature of basalts at Hawaiian volcanoes and Mt. Etna and within the

396   range of typical terrestrial basalts [1100 – 1250˚C, *Pinkerton*, 1987; *Harris and Rowland*, 2001;

397   *Vicari et al.*, 2007; *Harris and Rowland*, 2015].

398   4.2.3.   Self-replicating lava flow model

399   Many of the lava flows observed in the major Martian volcanic provinces of Tharsis and

400   Elysium display a similar repetitive morphology. *Baloga and Glaze* [2008] termed these flows

401   "self-replicating lava flows" and identified a set of defining criteria: morphologic characteristics

402   that repeat over the length of the flow, relatively constant channel and levee dimensions, and a

403   single channel that is visible for most of its length (Fig. 3). Their corresponding model of

404   propagation takes into account mass removed from the active molten lava flow during the

405   formation of lateral levees at the flow front as it propagates. The model assumes that levees are

406   created at the flow front due to a vertical parabolic velocity profile in the molten core consisting

407   of a Newtonian fluid, in which fluid at the top of the flow is traveling downslope faster than fluid

408   at its base (Fig. 4) [*Glaze and Baloga*, 2006; *Baloga and Glaze*, 2008]. The total excess flow

409   rate (Q_{ex}) that forms the levees is calculated as a product of the average excess flow velocity,

410   (u_c), width of the channel, and the thickness of the nondeformable crust atop the flow [*Baloga*

411   *and Glaze*, 2008, Eq. 10]. The excess mass is then left behind as the flow front advances at the

412   average downstream velocity of the molten core (u_c). Only a subset of lava flows in this study –

413   13 of 40 – met the *Baloga and Glaze* [2008] criteria of self-replicating flows.
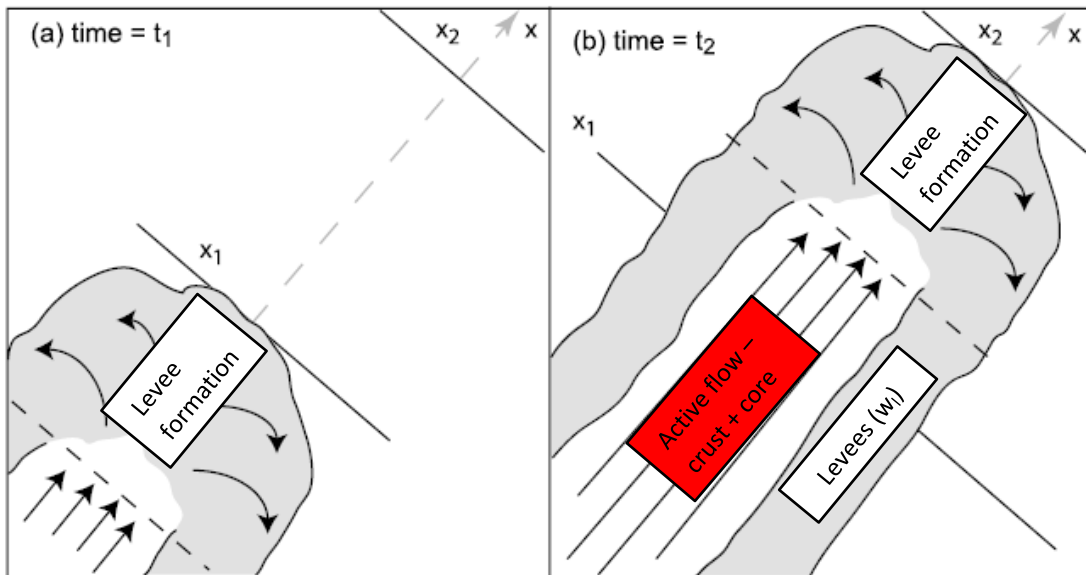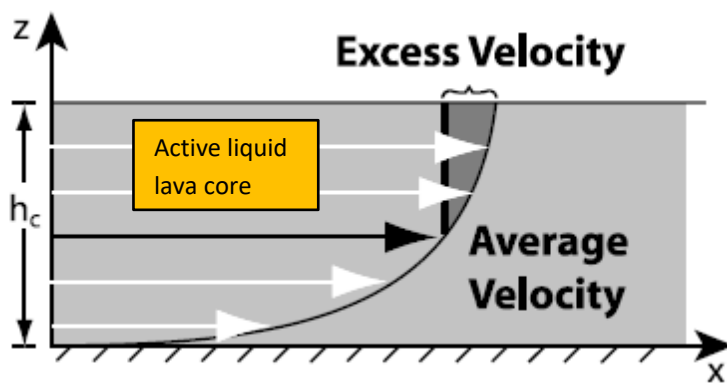
414
415 **Figure 3:** An example of a long, self-replicating lava flow in the volcanic plains of Tharsis
416 south of Olympus Mons. The channel is clearly defined, has an approximately constant width,
417 and levees are well developed and near constant width.

418

419   Using methods outlined in *Baloga and Glaze* [2008] and references therein, we

420 calculated eruption rates (Q) and the resultant viscosities and emplacement times for the 13

421 qualifying lava flows across the Tharsis Volcanic Province. To do so, we first calculated the

422 levee widths (w_l):

423

424 $$w_l = \frac{Q_{ex}}{u_c * h_l} \text{ (Eq. 6)}$$

425

426 where h_l is the levee thickness. Eq. (6) assumes that the excess volume flux Q_{ex} is u_c times the

427 dimensions of the levees, h_l and w_l. The crust thickness is assumed to be the difference between

428 total flow thickness and the liquid core thickness (h_c). The total flow thickness is approximated

429 by the height of the levees, such that the crust thickness is $h_l - h_c$. Crust thickness was found as a

430   function of distance downstream and the data was smoothed as in *Baloga and Glaze* (2008)

431   reaching an asymptotic value [Eqs. 12 & 13, Figure 8]. A cooling time for the asymptotic crust

432   thickness to form was calculated using solidification by radiant cooling following *Hon et al.*

433   [1994]. The emplacement duration of the flow was assumed to be the same as the time required

434   for crustal growth. Average effusion rate was calculated for each flow using its total volume and

435   the emplacement time.

436

437

438   **Figure 4:**   Modified from *Baloga and Glaze* [2008] illustrating how "self-replicating" lava
439   flows, which include well-defined channels and levees of relative constant width, are produced.
440   As the flow passes a given point, some mass of the flow at the flow front is deposited to form
441   levees.

442

443   2.2.4 Yield strength calculation

444   Our use of Eqs. 1 and 2 above assume Newtonian behavior, allowing viscosity to be

445 calculated from Jeffrey's equation (Eq.2). However, many suggest that most lavas, especially

446 those cooling during emplacement, behave as Bingham fluids [e.g., *Moore*, 1978]. In order to

447 explore this rheology further, we estimate the yield strength (σ) of each flow using underlying

448 slope (α), flow thickness (h), and an assumed lava density of 2700 kg m^{-3} (following the

449 procedure of *Heisinger* et al. 2007 and references therein).

450

451 $$\sigma = \rho g \sin(\alpha)\, h \quad \text{(Eq. 7)}$$

452

453 **5. Results**

454   5.1. Classification of Qualitative Flow Morphologies

455   5.1.1.   Channelized flows – high Ψ

456   Channelized lava flows – a common feature of either high-volume eruptions or flows

457 emplaced on steep slopes – are widely observed on the plains and shield volcanos of the Tharsis

458 volcanic province [e.g., *Carr*, 1973, 1974; *Greeley and Spudis*, 1981; *Baloga and Glaze*, 2008].

459 These flows are characterized by clearly defined (usually wide) channels and prominent levees

460 (Fig. 5a). The sources of these flows are obscured by the superposition of later flows and the

461 termination of the flow is marked by a reduction of channel visibility and the fanning out of the

462 flow into a smooth, featureless flow surface. Of the 40 lava flows in this study, 27 are

463 considered channelized flows. Thirteen of these flows display the self-replicating morphology

464 described in *Baloga and Glaze* [2008]. Channelized lava flows tend to be smaller in length and

465 width on central volcanoes than in the volcanic plains, and generally appear to correspond to the

466   high Ψ regime and, in the lab, are produced on slopes >5˚ or on shallower slopes at high eruption

467   rates [*Peiterson and Crown*, 1999; *Gregg and Fink*, 2000; *Peters*, 2020].

468   5.1.2.   Corrugated (folded) flows – intermediate Ψ

469   Corrugated flows – which are analogous to the fold morphology observed in PEG wax

470   experiments performed in the laboratory – are a variation of channelized flows [*Fink and*

471   *Griffiths,* 1990, 1992; *Gregg and Fink*, 2000]. Typically, these flows display a broad, open

472   channel and clearly defined levees. However, the inside of the channel and terminus of the flow

473   is characterized by a corrugated surface texture (Fig. 5b), interpreted to be the physical

474   manifestation of compression ridges on the surface crust. This texture has also been observed on

475   submarine and subaerial terrestrial flows. In this study, these flows are observed on Olympus

476   Mons and in the volcanic plains surrounding Ascraeus Mons. Of the 40 lava flows observed in

477   this study, five display this morphology. Of those five, four display a transitional morphology

478   between channelized and corrugated flows. The same behavior has been observed in the

479   laboratory and, in those cases, intermediate Ψ value ranges corresponding to transitional

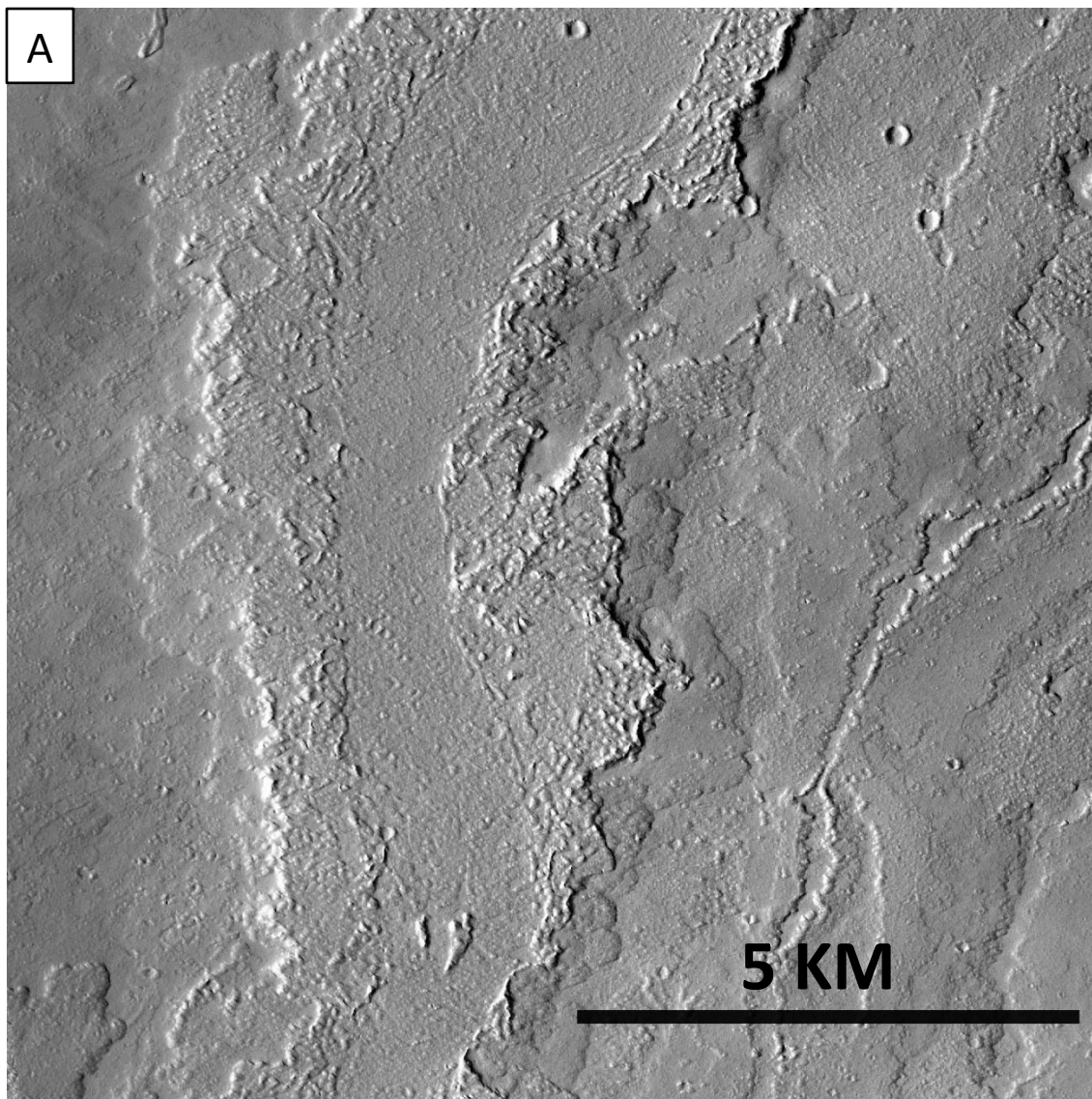480   morphologies were assigned [*Fink and Griffiths,* 1990, 1992; *Gregg and Fink*, 2000].

481   5.1.3.   Smooth flows – very high or low Ψ morphology
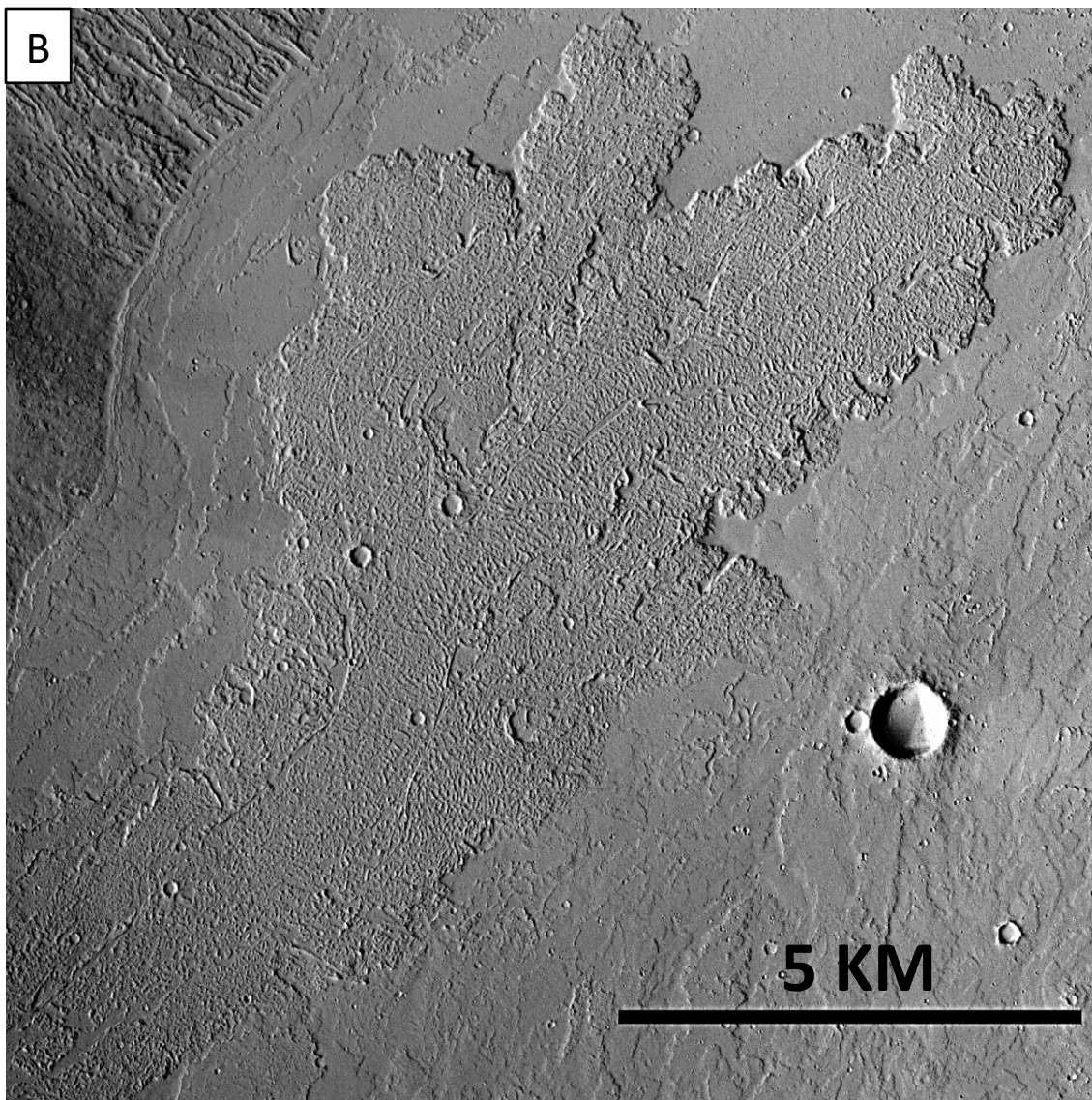
482   Many lava flows on Mars display a smooth, featureless texture that some believe

483   represent sheet flows emplaced by high eruption rates and/or low viscosity lavas, although some

484   of these flows might instead represent inflated pahoehoe flows [e.g., *Hon et al.*, 1994; *Bleacher*

485   *et al.*, 2017]. In our study, we avoided entirely smooth lava flows due to an inability to

486   distinguish between those flows which might represent wholesale emplacement at high eruption

487   rates and those which might have been emplaced as pahoehoe flow fields that have undergone

488   inflation. Nonetheless, two of the flows in our study, found in the volcanic plains, display

489   smooth textures along certain lengths of the flow. In these instances, a long-channelized portion

490   of the flow is also observed, and we therefore interpret these flows as transitional between

491   channelized and sheet flows corresponding to high / very high Ψ values.
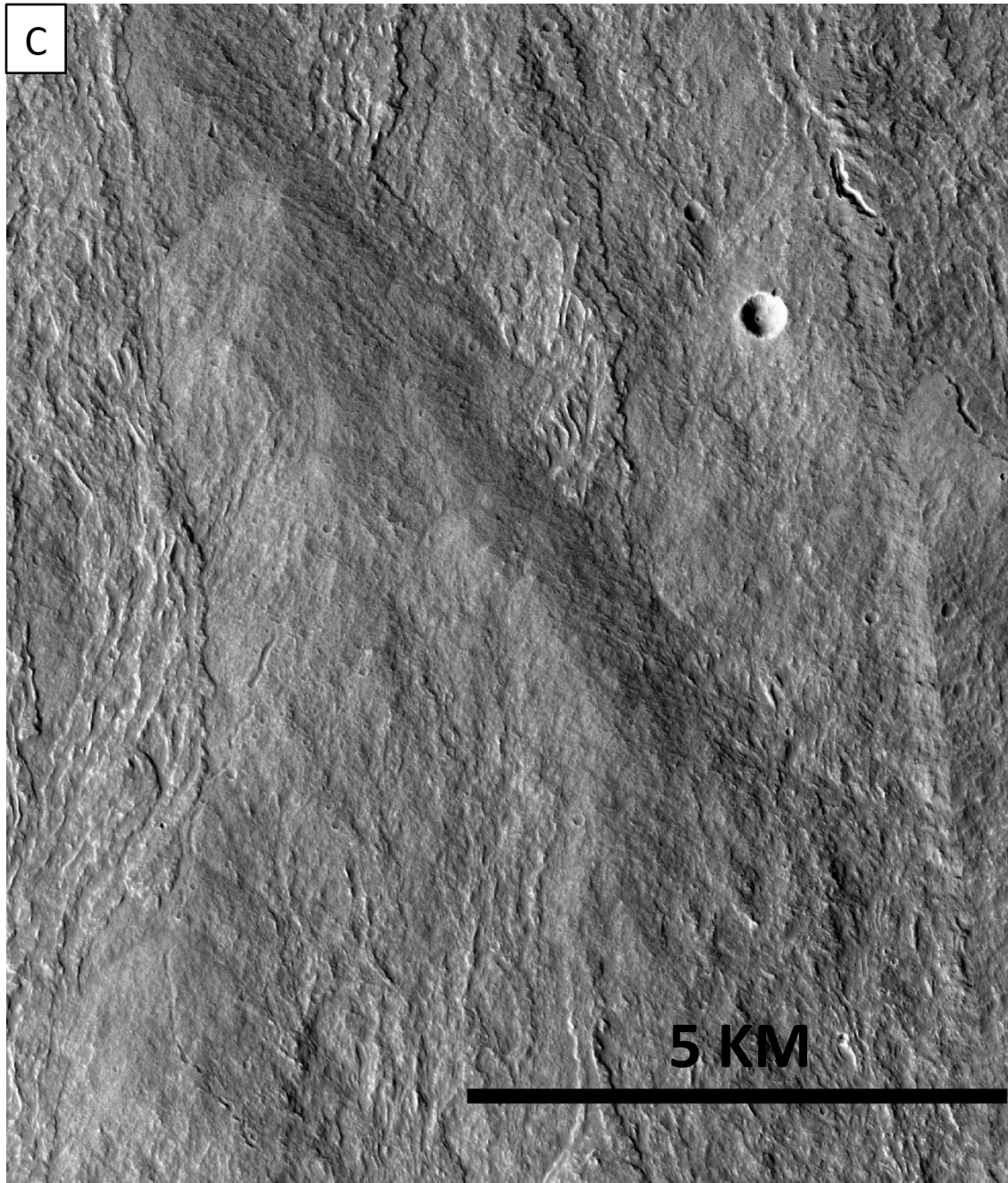
492   5.1.4.   Lava ridge flows – low Ψ on slopes

493   Lava ridges have been observed on and around central volcanoes, specifically Alba

494   Mons, Olympus Mons, and in the apron associated with Ascraeus Mons [*Sakimoto et al.*, 1997;

495   *Bleacher et al., 2007*]. These features have been interpreted as tube-fed flows, or lava tubes.

496   Lava ridges generally produce a broad triangular shaped rise in cross-section. Skylights are

497   observed on some of the ridges, where portions of the roof have collapsed into the void space

498   below. We interpret the tube-fed flows as being associated with low Ψ values, since analogous

499   features have been reproduced in the lab on a slope at low Ψ values. Six of the 40 studied flows

500   are classified as lava ridges.

502

Figure 5: Examples of the three predominant flow morphologies observed in this study. (a) channelized flow (b) corrugated flow (c) ridge flow. North is up in all images. The channelized flow has likely experienced drain out leaving behind a relatively smooth inner channel and raised levees. The ridge flow is likely a channelized flow that has roofed over – a tube-fed flow. Ridge flows are observed on Olympus Mons, Ascraeus Mons, and Alba Mons [*Sakimoto* et al., 1997; *Bleacher* et al., 2007]

5.2. Flow geometries

512   We measured the dimensions – length, width, and thickness – of 40 lava flows in the

513   Tharsis volcanic province on Mars. Using these flow dimensions, we calculated flow volumes.

514   Flows occurred in three subregions: on central volcanoes (i.e. Olympus Mons and Ascraeus

515   Mons apron), in close proximity to central volcanoes (i.e. Olympus Mons and Ascraeus Mons),

516   and in the volcanic plains of Tharsis. The 40 lava flows ranged in length from ~15 to 314 km.

517   The longest flows occurred in the volcanic plains. Mean flow widths ranged from ~0.5 to 29 km,

518   with the narrowest flows occurring on Olympus Mons. Flow thicknesses ranged from ~11 to 91

519   m. Flow areas and volumes ranged from ~14 to 11,180 km^2 and ~1 to 430 km^3, respectively.

520   The smallest flows in areal extent and volume are observed on Olympus Mons and Ascraeus

521   Mons apron, while the largest flows occur in the volcanic plains of Tharsis surrounding the

522   Tharsis Montes and Daedalia Planum. The lava flows were emplaced on slopes ~0.3 – 6.6˚, with

523   the steepest slopes occurring on the flanks of Olympus Mons. Slopes in the volcanic plains

524   typically ranged from ~0.3 to 1˚.

525   5.3. Rheological analyses

526   The methods described above in 4.2.1 were applied to 34 of 40 lava flows. Resulting

527   volumetric flow rates, or effusion rates ranged from 3×10^2 to ~3.5×10^4 m^3/s (Table 2). Higher

528   effusion rates were estimated for the intervolcanic plains and Daedalia Planum, while lower

529   effusion rates were estimated for flows on Olympus Mons. We calculated effective flow

530   viscosities of ~10^4 – 10^7 Pa s and yield strengths of ~800 – 3×10^4 Pa. Viscosities and yield

531   strengths were highest for flows observed on Olympus Mons and lowest for those in the volcanic

532   plains. Modeled emplacement times for the lava flows ranged from 9 days to ~1 year.

533

CALCULATIONS USING GRAETZ NUMBER AND JEFFREY'S EQUATION

FLOW #	Eruption Rate (m³/s)	Viscosity (Pa-s)	Yield Strength (Pa)
1	1680	9.4×10^4	7.7×10^2
2	16330	2.1×10^6	3.1×10^3
3	34781	9.4×10^5	2.2×10^3
4	60	7.4×10^7	3.1×10^4
5	245	1.4×10^6	1.3×10^4
6	342	3.3×10^7	1.8×10^4
7	3981	7.9×10^5	2.0×10^3
8	2855	1.4×10^5	9.3×10^2
9	2761	1.4×10^6	3.1×10^3
10	3654	2.5×10^6	4.3×10^3
11	3994	6.9×10^6	4.0×10^3
12	17113	4.6×10^6	6.0×10^3
13	11859	9.0×10^5	3.0×10^3
14	5646	1.3×10^6	3.8×10^3
15	3496	1.6×10^5	2.0×10^3
16	4981	1.6×10^5	2.8×10^3
17	4190	2.0×10^5	1.9×10^3
18	656	9.5×10^5	2.0×10^3
19	2145	1.2×10^6	3.5×10^3
20	4816	3.8×10^6	3.3×10^3
21	7881	3.4×10^6	3.4×10^3
22	152	1.1×10^7	1.4×10^4
23			
24	298	7.0×10^6	1.5×10^4
25			
26			
27			
28			
29			
30	1612	3.0×10^6	2.3×10^3
31	255	2.0×10^7	7.5×10^3
32	2255	2.8×10^6	3.4×10^3
33	2151	3.2×10^6	4.1×10^3
34	1585	1.3×10^6	2.8×10^3
35	2875	2.1×10^5	2.2×10^3
36	395	1.6×10^5	1.3×10^3

37	824	2.1×10^5	1.7×10^3
38	5579	1.8×10^5	1.7×10^3
39	3107	7.0×10^5	1.9×10^3
40	8242	9.7×10^6	5.8×10^3

Table 2: Eruption rates and rheological properties of 34 lava flows on Mars using a Graetz number of 300 and Jefferey's equation. Blank cells represent lava ridges, whose eruption rates cannot be estimated based on their morphology.

5.4. Application of Ψ

We used assigned Ψ value*s* to calculate eruption rates and emplacement times for all 40 lava flows. Assuming a solidification temperature of 900˚C and an eruption temperature of 1150˚C, calculated effusion rates using Eqs. 3 and 4 ranged from 0.2 – 6500 m³/s (Table 3). Effusion rates corresponding to each morphology are: smooth-levee flows (~6500 m³/s); levee flows (950 – 6500 m³/s); levee-fold flows (575 – 950 m³/s); folded flows (35 – 575 m³/s); rift, or tube-fed, flows (0.2 – 20 m³/s). The kinematic viscosity was an input instead of an output in this model, and we used a value of ~10^2 Pa s [*Nichols*, 1939; *Hon et al.*, 1994;]. Yield strengths are not an output of Ψ and were not calculated via this method. Emplacement times range from ~14 hours –2200 years. The largest emplacement times (180 – 2200 years) were exclusively for the lava ridge flows and were calculated using the lowest effusion rate of the range – 0.2 m³/s. If the higher end of the range for lava ridges is used (20 m³/s), the emplacement times for lava ridges are 1.8 – 22 years. If lava ridges are removed, the emplacement times range from ~14 hours – 9.5 years.

APPLICATION OF Ψ	
FLOW #	**Eruption Rates (m³/s)**
1	950 - 6500
2	950 - 6500
3	6500
4	575 - 950
5	575 - 950

6	950 - 6500
7	950 - 6500
8	950 - 6500
9	950 - 6500
10	950 - 6500
11	575 - 950
12	950 - 6500
13	950 - 6500
14	950 - 6500
15	575 - 950
16	950 - 6500
17	950 - 6500
18	35 - 575
19	950 - 6500
20	950 - 6500
21	6500
22	950 - 6500
23	0.2 - 20
24	950 - 6500
25	0.2 - 20
26	0.2 - 20
27	0.2 - 20
28	0.2 - 20
29	0.2 - 20
30	950 - 6500
31	950 - 6500
32	950 - 6500
33	950 - 6500
34	950 - 6500
35	950 - 6500
36	950 - 6500
37	950 - 6500
38	950 - 6500
39	950 - 6500
40	950 - 6500

552   **Table 3**: Eruption rate ranges for 40 lava flows on Mars by based on surface morphology,
553   assigned Ψ value, and assumed ambient and flow properties.
554

555   5.5. Self-replicating lava flow model

556   The self-replication model as outlined by *Baloga and Glaze* [2008] was applied to 13

557   qualifying flows to calculate effusion rates and emplacement times as described above.

558   Viscosities were then calculated by treating the lava as a Newtonian fluid and using Jeffrey's

559   equation (Eq. 2). Yield strengths were calculated by treating the flow as a Bingham fluid (Eq.

560   4). Modeled effusion rates are ~30 – ~1200 m³/s (Table 4). Eruption rates were highest for lava

561   flows observed in the volcanic plains. Viscosities ranged from 4.5×10^6 – $\sim 3 \times 10^7$ Pa s and

562   yield strengths ranged from $\sim 10^3$ Pa – 3.6×10^4 Pa. The time of emplacement for these flows

563   ranges from 4.5 months – 9 years. No appreciable difference in viscosity or emplacement time

564   was observed between the Tharsis subregions.

SELF-REPLICATION LAVA FLOW MODEL
[BALOGA & GLAZE, 2008]

FLOW #	Yield Strength (Pa)	Eruption Rate (m³/s)	Viscosity (Pa-s)
1			
2	3.4×10^3	1174.39	9.5×10^6
3	5.3×10^3	335.62	2.9×10^7
4			
5			
6			
7			
8			
9			
10	4.6×10^3	52.66	3.2×10^7
11			
12			
13			
14	3.3×10^3	135.42	2.0×10^7
15			
16			
17			
18			
19			
20			
21	7.9×10^3	285.09	1.5×10^7
22	1.7×10^4	27.60	2.9×10^7
23			
24	3.6×10^4	26.90	1.5×10^7
25			

26			
27			
28			
29			
30	1.4×10^3	46.00	1.7×10^7
31			
32	2.7×10^3	236.21	1.6×10^7
33	4.0×10^3	204.30	2.2×10^7
34	2.0×10^3	50.57	1.0×10^7
35	2.8×10^3	89.26	2.5×10^6
36			
37			
38			
39	1.4×10^3	111.17	4.5×10^6
40			

565 **Table 4:** Eruption rates and rheologic properties of 13 lava flows on Mars using the self-
566 replication model for long lava flows [*Baloga and Glaze*, 2008].
567

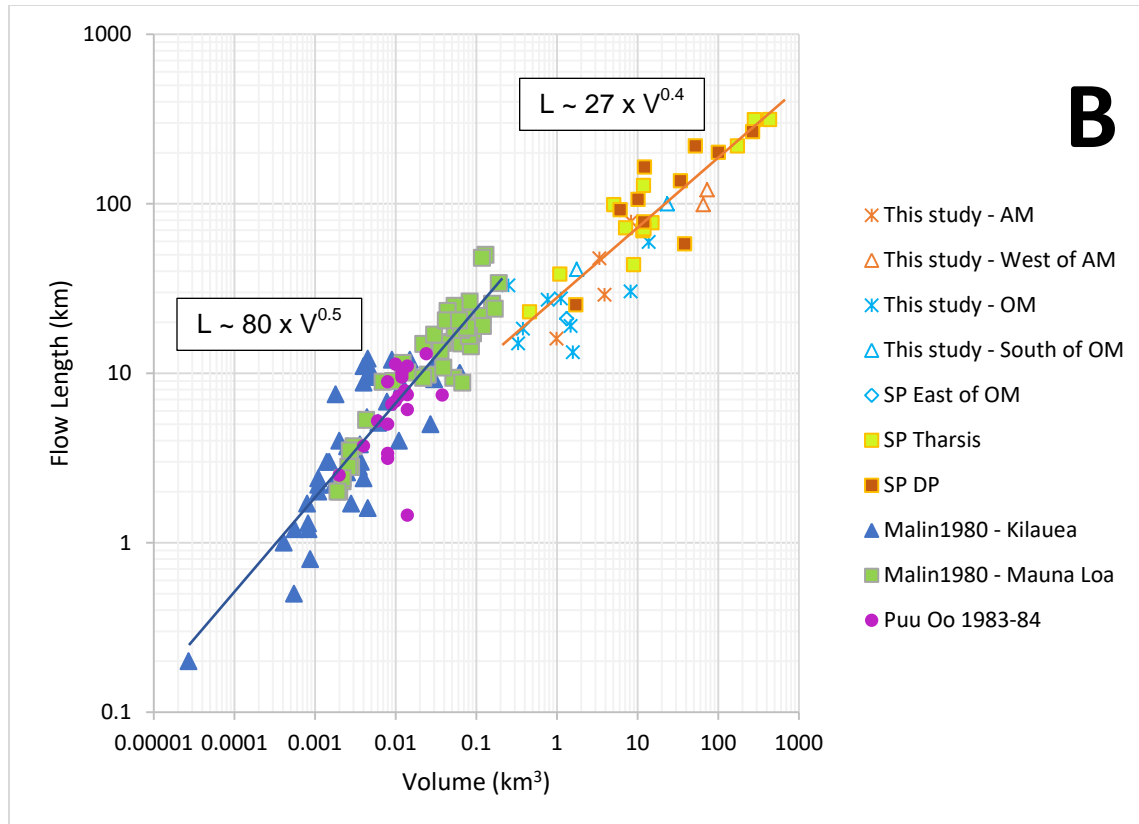568 **6. Discussion and Implications**

569 6.1. Martian volcanism

570 6.1.1. Volumes, extent, and distribution of lava flows

571 Martian volcanism has decreased in spatial extent and frequency. According to a number

572 of studies that have used crater counts, geomorphology, and modelling, the bulk of Martian

573 volcanism occurred >3 Ga during the Noachian and Early Hesperian [e.g. *Plescia*, 2004; *Werner*,

574 2009; *Tanaka et al.*, 2014]. Early volcanic activity consisted of plains-style volcanism, possible

575 explosive eruptions, and the construction of the large shields [e.g., *Carr*, 1973, 1974; *Plescia*,

576 2004]. As Mars has cooled over time, the number of volcanoes erupting and the volumes of

577 erupted magma have decreased [e.g., *Greeley and Spudis*, 1981; *Bleacher et al.*, 2007; *Werner*,

578 2009; *Xiao et al*., 2012]. The flows in our study are among the most recent examples of effusive

579 volcanism in the Tharsis Volcanic Province and on Mars. Studies by *Tanaka et al*. [2014] and

580 *Werner* [2009] suggest that these flows were emplaced in the Late Amazonian and range in age

581   from 10s – 100s of millions of years old. There is some variability in age among sub-regions

582   within Tharsis. The flows on the flanks of Olympus Mons and Ascraeus Mons are ~100 – 700

583   Ma and 100 – 800 Ma, respectively, with localized areas < 50 Ma while the aprons emanating

584   from Ascraues Mons aprons are ~1 Ga [e.g., *Neukum et al.*, 2004; *Werner*, 2009], compared to

585   the flows in the volcanic plains that likely range in age from <100 to 400 Ma [e.g. *Hauber et al.*,

586   2011]. The volumes of eruptions are also less on Olympus Mons and the Ascraues Mons apron

587   relative to the volcanic plains [*Bleacher et al.*, 2007; this study].

588

589
Figure 6: Volumes are expressed as a function of flow length and area covered. AM = Ascraeus Mons; OM = Olympus Mons; DP = Daedalia Planum; CRB = Columbia River Basalts. **(a)** The calculated volumes and area covered of the 40 lava flows observed in this study are plotted along with the 1983-1984 Pu'u O'o lava flows [*Wolf* et al., 1987] and Columbia River Basalt [*Self* et al., 1997]. The smallest flows are not too dissimilar to the Pu'u O'o lava flows, while the largest flows are similar in size and volume to those erupted in the Columbia River basalts. **(b)** Measured flow length is plotted as a function of calculated volume for 40 lava flows on Mars and are compared to terrestrial flows in Hawai'i. The bulk of Martian flows are longer and volumetrically larger, however, a subset of flows primarily related to central volcanoes overlap in length with Mauna Loa flows. Power law relationships (blue line – terrestrial; orange line – Mars) for Hawaiian lava flows are compared to the Martian lava flows. According to *Malin* [1980], an exponent equal to 0.5 indicates both length and cross-sectional area of the flows are controlled by volume. The Mars lava flows have an exponent ~0.4 indicating length and cross-sectional area are largely controlled by volume.

604

605   Figure 6a shows the area covered by our flows in km² versus their volumes in km³. In

606   terms of volume and corresponding area, flows on the central volcanoes of Ascraeus Mons (AM)

607   and Olympus Mons (OM) (denoted by stars) are distinct from and smaller than flows associated
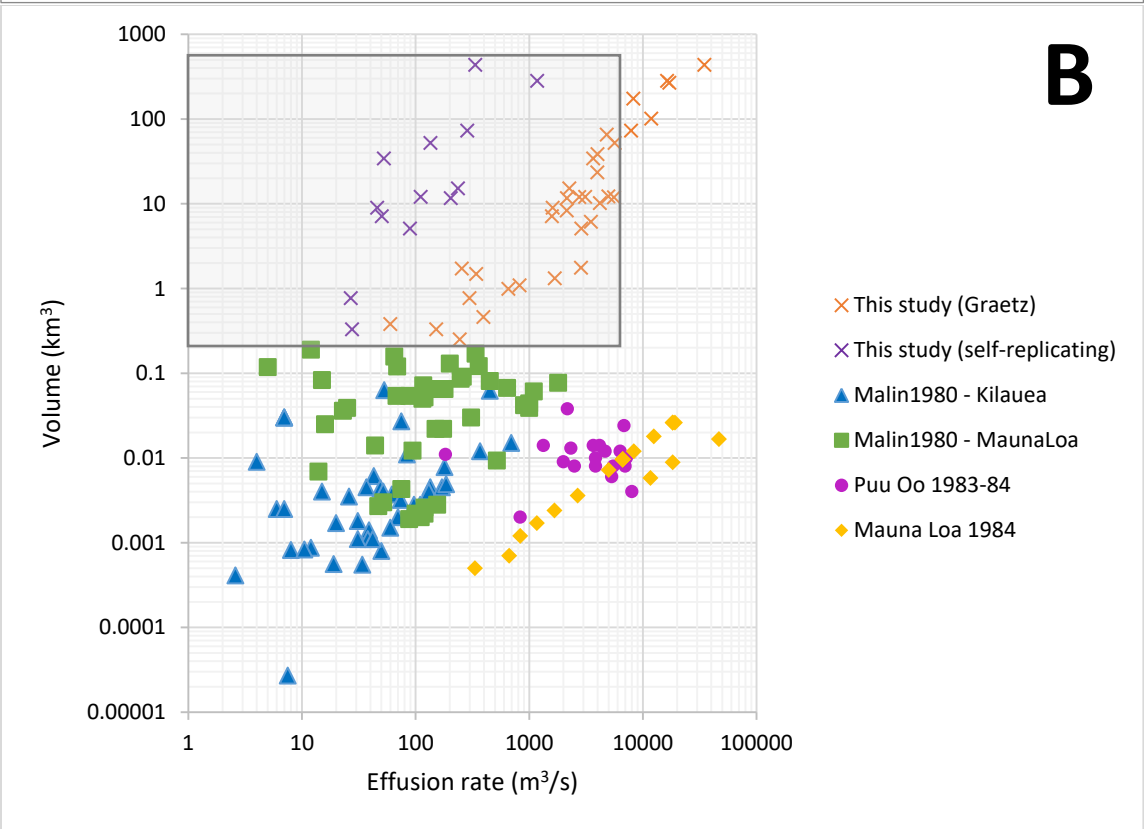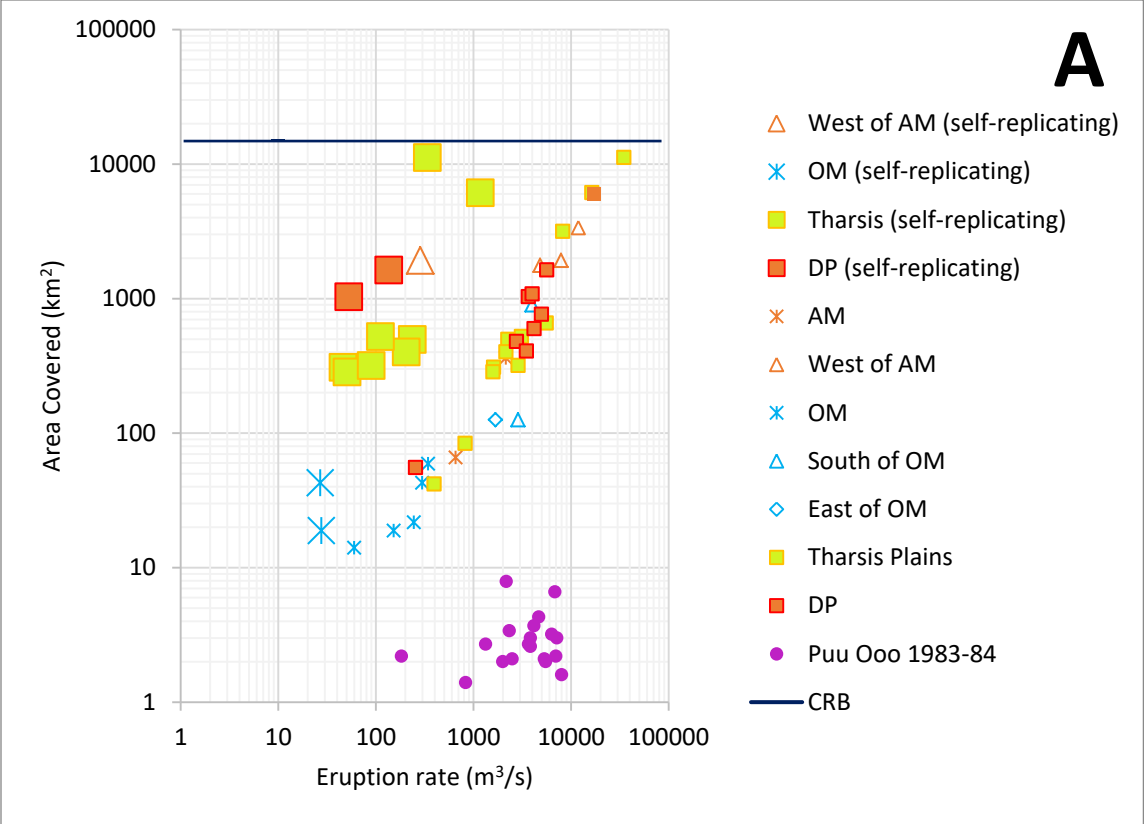
608   with plains volcanism (squares). A similar relationship can be seen in Figure 6b where lava flow

609   length (km) is shown against total volume.
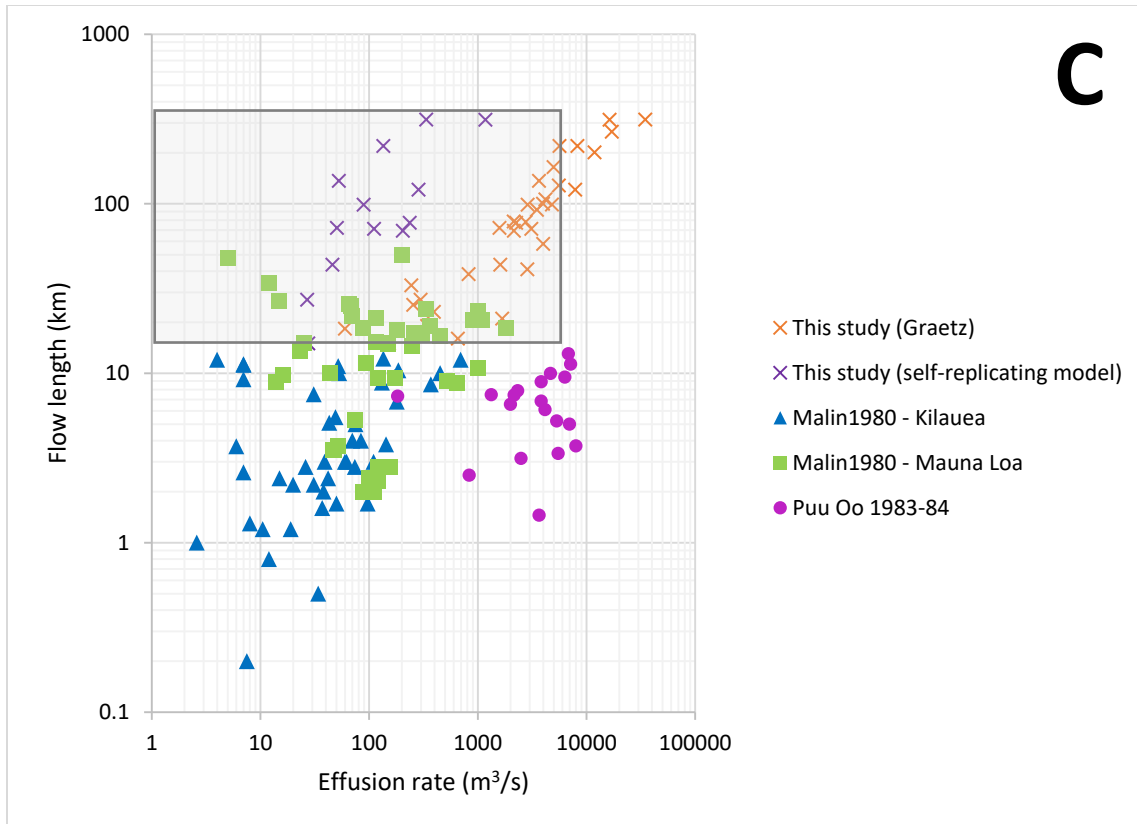
610   In Figure 6a, we also compare the Mars flows to well-documented terrestrial flows. We

611   first note that in terms of volume / area, the Mars flows follow the same trend as terrestrial flows

612   and sit directly between Hawaiian flows [Pu'u O'o, 1983-84, *Wolfe et al*., 1987] and flows from

613   the Columbia River Basalts [CRB, *Self et al*., 1996]. Further, the OM and AM flows sit close to

614   the Pu'u O'o flows whereas the plains flows extend over a greater range, reaching but not

615   overlapping with the CRB flows. We also note that the plains flows are longer than flows

616   erupted from central vents (Fig. 6b).

617   In Figure 6b, we note that the relationship between volume and length follows a power

618   law for both terrestrial and Mars flows. The terrestrial flows follow a relationship with a power-

619   law exponent of roughly 0.5. According to *Malin* [1980] a power-law exponent of 0.33 would

620   indicate that flow length, width, and depth are equally controlled by (and proportional to) the

621   volume erupted, whereas an exponent of 1 would indicate that the cross-sectional area of the

622   flow does not vary with volume, and thus only the length is controlled by volume. *Malin* [1980]

623   interprets the exponent of 0.5 to indicate that both the length and cross-sectional area (product of

624   thickness and width) of the flows are controlled by the volume, and that length and cross-

625   sectional area are mutually dependent. The Mars flows can be fitted by an exponent close to 0.4,

626   again suggesting that volume controls both length and cross-sectional area, with the <0.5

627   exponent of the Mars flows possibly reflecting their wide range of substrate slopes and

628   viscosities that also control flow geometry in complex ways.

629   6.1.2 Model Results: effusion rate, duration, and rheology

630   Our calculated effusion rates allow differentiation among the subregions (Figure 7a), with

631   the highest rates estimated for the plains regions (squares) and the lowest values estimated for

632   Ascreaus and Olympus Mons (stars). Regions located between central volcanoes and volcanic

633   plains (triangles) have intermediate effusion rates. The application of the halting Graetz number

634   ($G_z = 300$) and the self-replicating model of *Glaze and Baloga* [2008] produce eruption rates for

635   Ascreaus and Olympus Mons that match well to terrestrial values despite the much greater

636   volumes of the Mars flows (Fig. 7b, c, orange vs. purple Xs). Eruption rates for the plains

637   regions on Mars exceed many Hawaiian eruption rates but are consistent with some of the

638   highest eruption rates measured at the Pu'u O'o vent [1983-84, *Wolfe et al.*, 1987] and Mauna

639   Loa [1984, *Lipman and Banks*, 1987]. Lower eruption rates are estimated when flow

640   morphology and mass allocation to levees are taken into account in the self-replicating model

641   [Fig. 7; *Glaze and Baloga*, 2006; *Baloga and Glaze*, 2008]. Eruption rates obtained using Ψ

642   morphologies span nearly the entire range of available terrestrial values and those obtained by

643   the two other models, with the exception of the uppermost values calculated by assuming a
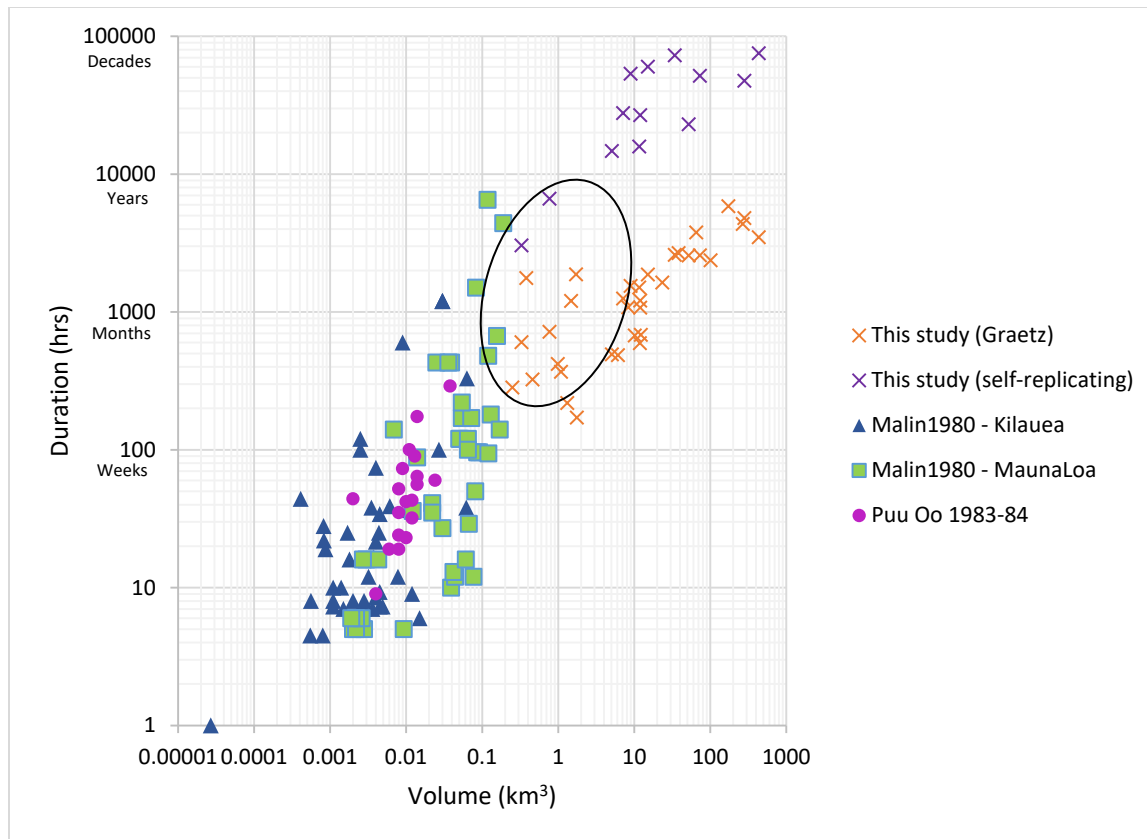
644   halting $G_z = 300$.

Figure 7: AM = Ascraeus Mons; OM = Olympus Mons; DP = Daedalia Planum. **(a)** Relationship between eruption rate and area covered. The Mars flows are compared to flows erupted during the 1983-84 Pu'u O'o eruption in Hawai'i and the Columbia River Basalts (CRB). Large symbols denote values derived using self-replication model for long lava flows. Small symbols indicate values calculated using Graetz number. Stars indicate values obtained for central volcanoes. Navy blue line denotes minimum areal extent of CRB flows from *Self et al.* [1997]. This data supports the conclusion that eruption rates are controlled by subregions, with higher eruption rates calculated for the volcanic plains than central volcanoes. In general, the self-replication model produces lower eruption rates than using the Graetz number. **(b)** The relationship between eruption rate and total erupted volume. The eruption rates for the Mars lava flows are comparable to terrestrial values. The highest eruption rates calculated for Mars are similar to the highest values observed on Earth during the Mauna Loa eruption of 1984. Although the lower volume estimates are similar to those observed on Mauna Loa, most of the flow volumes are 2 – 4 orders of magnitude greater. **(c)** Figured modified from *Walker* [1973]. Log-log plot shows the length of lava flows as function of the eruption rate for terrestrial lava flows at Mauna Loa and Kilauea. Superposed on that figure are the eruption rates calculated using the three models in this study. Orange X's are calculated eruption rates using Graetz number. Purple X's are eruption rates calculated from self-replication model. Shaded gray box represents ranges of eruption rates calculated using Ψ.

The flows on Olympus Mons are smaller than those observed in the volcanic plains of

Tharsis and tend to be open channel flows, which may suggest short-lived, volume-limited

670   eruptions [*Bleacher et al.*, 2007]. The flows in the volcanic plains are larger in areal extent than

671   flows observed on Olympus Mons or the Ascraeus Mons apron. The variability in flow volume

672   by subregion suggests different eruption conditions, specifically differences in subsurface

673   pathways and magma sources. The volumetrically larger flows were likely erupted to the surface

674   by large dikes and remained active for long periods of time (Fig. 8), consistent with findings of

675   *Wilson and Head* [1983]. Meanwhile, the flows on Olympus Mons and proximal to Ascraeus

676   Mons were likely emplaced by smaller subsurface conduits that were active for shorter periods of

677   time consistent with findings of *Bleacher et al.* [2007] and *Wilson and Head* [1983]. We also

678   note that the largest of the Mars flows, given the measured volumes and calculated eruption

679   rates, must have been active much longer than typical terrestrial flows from places like Hawaii

680   (Fig. 8), but may rather be akin to regions like the Columbia River Basalts which are thought to

681   have been active over long periods to generate voluminous fields; this is particularly likely for

682   the Mars plains volcanism characterized here [*Self et al*., 1996].

683
684 **Figure 8**: The calculated volume of Mars lava flows is compared to terrestrial flows as a
685 function of duration of emplacement. Black circle contains Mars flows associated with central
686 volcanoes, whereas remaining flows were produced in the plains. The Mars lava flows are much
687 larger in volume – although some values are similar to Mauna Loa – and erupted over greater
688 lengths of time. This suggests that feeder dikes and other pathways necessary to producing these
689 flows remained active and open for longer periods than pathways on Earth.
690

691   6.1.3 Comparison to previous work

692   Our results are generally consistent with other studies: *Hiesinger et al.* [2007] calculated

693 effusion rates for 25 young flows on the eastern flank of Ascraeus Mons, resulting in a range of

694 ~20 to ~400 m^3/s that falls within the range we calculated for nearby flows using all three

695 models. On the other hand, our effusion rates for the lava ridges, interpreted as tube-fed flows

696 (0.2 – 20 m^3/s) fall at the very low end of the range proposed by *Sakimoto et al.* [1997] of $2 – 10^5$

697 m^3/s. Despite the long runouts of lava flows in the Tharsis region of Mars, our analysis shows

698 that very high effusion rates of ~10^5 m^3/s are not required to explain the observed flows.
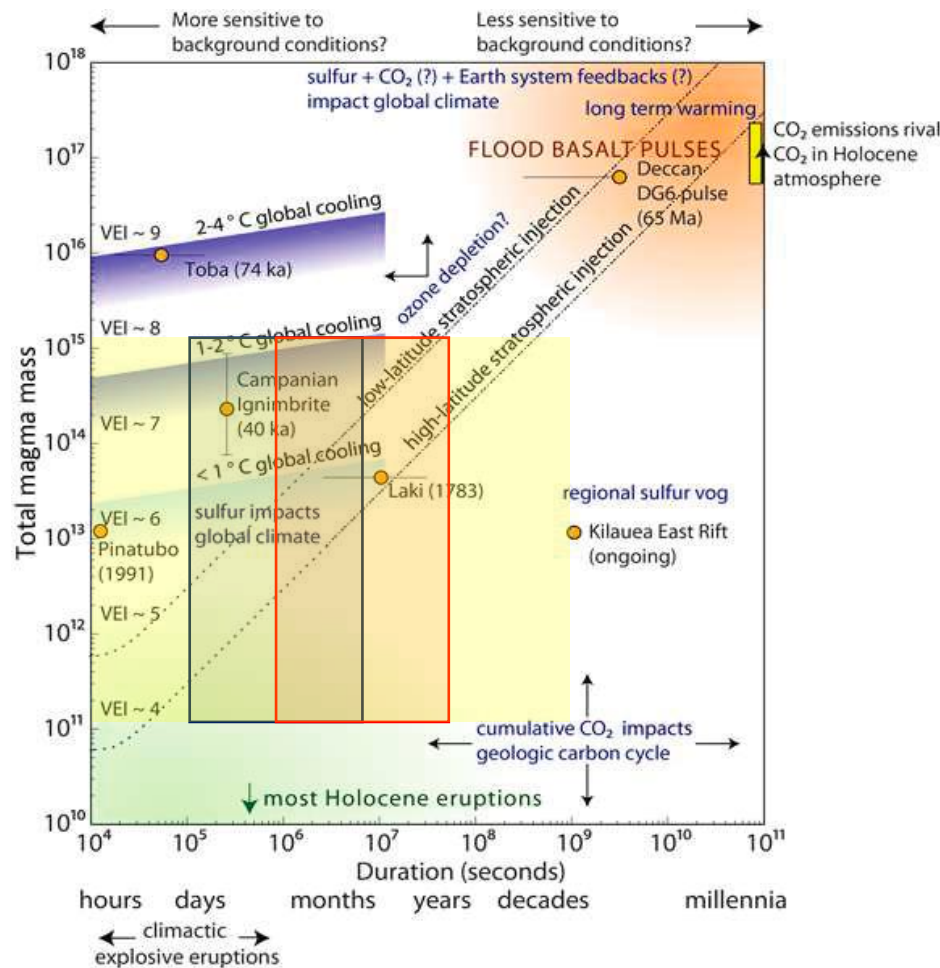
699   Earlier studies of Martian volcanism invoked ultramafic and other exotic compositions to

700   explain the large, voluminous effusive eruptions preserved across the surface of the planet [e.g.,

701   *Sakimoto et al*., 1997; *Cashman et al.*, 1998; *Garry et al*., 2007].   While the ranges differ

702   depending on the model, the viscosities of $10^4 - 10^7$ Pa s calculated in this study are consistent

703   with a basalt to basaltic andesite composition, which is observed on all dust-free Martian

704   surfaces [*Rogers and Christensen*, 2007].   These viscosities are similar to those calculated for the

705   25 young lava flows observed (10^4-10^7 Pa-s) by *Hiesinger* et al. [2007] and the 8 lava flows

706   observed in the volcanic plains of Tharsis (10^2-10^3 Pa-s) by *Hauber* et al. [2011].   In Hawaii,

707   recently erupted basalt has viscosities $\sim 10^2 - 10^3$ Pa s, similar to Mt. Etna ($\sim 10^3$) [e.g., *Self et al*.,

708   2008; *Harris and Rowland*, 2015].   The viscosity of some Columbia River Basalt and Deccan

709   Trap lavas has been estimated to be 500 and 100 Pa s at the time of emplacement [e.g., *Self et al*.,

710   1997; 2008].

711   The rheologic model results in slightly lower calculated viscosities, due to the estimate of

712   effusion rate (Q) which could be an order of magnitude higher than reality because it assumes the

713   entire flow front is active during the time of emplacement.   Jeffrey's equation is particularly

714   sensitive to the flow thickness.   The flow thicknesses measured in our study are taken to be the

715   maximum thickness, assuming erosion and gradation has not significantly altered the flow.   The

716   self-replication model produces viscosity values at the higher end of basalt ($10^6 - 10^7$ Pa s) and

717   more congruent with basaltic andesite or a highly crystallized basalt.   *Baloga and Glaze* [2008]

718   obtained a value of 10^6 Pa-s for one very long lava flow which is the same flow as our Flow 2,

719   for which we calculated $\sim 10^7$ Pa-s.   The difference is due to differing flow lengths: *Baloga and*

720   *Glaze* [2008] measured a 173 km flow length, whereas we measured 313 km for the same flow.

721   6.1.4   Planetary evolution & interior

722   Martian volcanism, although widespread early in its history, has become more localized

723   with time.   The most recent episodes of volcanism have occurred near the Elysium Mons

724   volcanic province around Cerberus Fossae and the Tharsis Volcanic Province [e.g., *Neukum et*

725   *al.*, 2004; *Werner,* 2009], with both provinces separated by thousands of kilometers.   The

726   effusion rates and viscosities of the most recent eruptions studied here (~10s – 100s Ma likely in

727   the plains, Figs. 8 and 9) suggests that Martian interior has produced eruptions on par with those

728   of flood basalts and large igneous provinces on Earth.   Our modeled durations (Fig. 9) imply that

729   a large supply of eruptible magma had an open pathway to the surface over long periods of time,

730   particularly in the volcanic plains [e.g. *Wilson and Head*, 1983].   Given the volumes calculated

731   in this study, these pathways would have been linked to sizeable magma bodies.   The

732   observation of relatively young low shields in the volcanic plains of Tharsis (<100 Ma) might

733   hint at a larger magma body, perhaps related to the proposed plume beneath Tharsis [e.g., *Dohm*

734   *et al.,* 2017].

Figure 9: Mass of martian flows and emplacement times are compared with notable terrestrial eruptions. Blue box represents Graetz number minimum eruption durations, while red box represents self-replication model eruption durations. Green box represents eruption durations for full range of Ψ derived eruption rates. Modified from Black and Manga [2017].

The contribution of effusive volcanism to climate has been a subject of open speculation for terrestrial and extraterrestrial systems, such that both total mass erupted and eruption duration play a role in controlling climate forcing [Figure 9; *Self et al.*, 1997; *Black and Manga*, 2017; *Rader et al.*, 2017]. Some of the eruptions represented by the lava flows in our study may have lasted for decades and the masses are on the order of very large terrestrial eruptions. The masses of individual flows calculated in our study are less than that of complete members in terrestrial large igneous provinces, but some, especially those in the plains, do overlap with other eruptions that had significant global impacts, consistent with up to 2 degrees of global cooling. While

749 large igneous provinces typically erupt over millions of years on Earth, the Tharsis volcanic

750 province has produced volcanic eruptions over billions of years [e.g*., Self et al.*, 1996; 1997;

751 2008; *Sheth,* 2006; *Werner*, 2009; *Tanaka et al.*, 2014], possibly enhancing their capacity for

752 atmospheric forcing. And, the high altitude of the eruptions at Tharsis may have further

753 enhanced their ability to produce climatic impacts [e.g., *Sheth*, 2006]. Whether or not those

754 eruptions were continuous or volumetrically significant enough to impact the atmosphere

755 remains an open question, although our analysis demonstrates that individual flows in Tharsis are

756 at the very least of the scale of large terrestrial eruptions that caused short term changes to global

757 climate.

7. Conclusions

759   This study produced volumes, effusion rates, viscosities, and emplacement times for 40

760 lava flows in the Tharsis Volcanic Province on Mars. The results have implications for recent

761 volcanism on Mars, lava composition, the plumbing of the Martian subsurface, and potential

762 climatic effects. Sub-regional differences in flow volumes across the Tharsis volcanic province

763 suggest different magma sources and subsurface plumbing conditions for central volcanoes and

764 lava plains. Drawing from these analyses, we conclude the following:

765   **1.** Martian lava flows do not require extremely high volumetric flow rates or exotic lava

766   compositions. Observed lava flows can be produced by terrestrial volumetric flow

767   rates and non-exotic lava compositions with viscosities and yield strengths suggestive

768   of basalt and basaltic andesite compositions.

769   **2.** Subsurface pathways in the Martian interior were long-lived and capable of erupting

770   melts for months to years in some cases producing individual lava flows of

771   remarkable length and volume. Additionally, if the ages of the flows are accurate,

magma was being stored and transported throughout the Martian crust from the mantle within the last 1 Ga – and as recent as ~10 – 100 Ma during the Late Amazonian.

3. Olympus Mons has produced volumetrically smaller recent eruptions than sources of lava flows in the volcanic plains, suggesting smaller dikes and possibly a smaller, secondary magma source within Olympus Mons. The volcanic plains may be fed directly through a thinner overlying crust by a more abundant source related to a mantle plume or a young plume head.

4. Given the volume of some erupted flows, it is possible that the corresponding volcanic activity impacted the Martian climate, but whether or not those impacts were regional or global, short-term or long-term is unknown.

789

8. References

790

791 Baloga, S.M., and L.S. Glaze (2008), A self-replication model for long channelized lava flows

792   on the Mars plains, *J. Geophys. Res.*, 113, E05003, doi: 10.1029/2007JE002954.

793 Baloga, S.M., Glaze, L.S., Crisp, J.A., and S.A. Stockman (1998), New statistics for estimating

794   the bulk rheology of active lava flows: Puu Oo examples, *J. Geophys. Res.*, 103, No. B3,

795   5133–5142.

796 Black, B.A., and M. Manga (2016), The eruptibility of magmas at Tharsis and Syrtis Major on

797   Mars, *J. Geophys. Res. Planets*, 121, 944–964, doi: 10.1002/2016JE004998.

798 Black, B.A., and M. Manga (2017), Volatiles and the tempo of flood basalt magmatism, *Earth*

799   *Planet. Sci. Lett.*, 458, 130–140.

800 Bleacher, J.E., Greeley, R., Williams, D.A., Werner, S.C., Hauber, E., and G. Neukum (2007),

801   Olympus Mons, Mars: Inferred changes in late Amazonian aged effusive activity from lava

802   flow mapping of Mars Express High-Resolution Stereo data, *J. Geophys. Res., 112,* E04003,

803   doi: 10.1029/2006JE002826.

804 Bleacher, J.E., Greeley, R., Williams, D.A., Cave, S.R., and G. Neukum (2007), Trends in

805   effusive style at the Tharsis Montes, Mars, and implications for the development of the

806   Tharsis province, *J. Geophys. Res.*, 112, E09005, doi: 10.1029/2006JE002873.

807 Bleacher, J.E., Orr, T.R., de Wet, A.P., Zimbelman, J.R., Hamilton, C.W., Garry, W.B.,

808   Crumpler, L.S., and D.A. Williams (2017), Plateaus and sinuous ridges as the fingerprints of

809   lava flow inflation in the Eastern Tharsis Plains of Mars, *J. Volcano. Geotherm. Res.*,

810   http://dx.doi.org/10.1016/j.jvolgeores.2017.03.025.

811 Bruno, B.C., Baloga, S.M., and G. J. Taylor (1996), Modeling gravity-driven flows on an

812   inclined plane, *J. Geophys. Res.*, 101, No. B5, 11,595–11,577.

813   Byrne, P.K., B. van Wyk de Vries, J.B. Murray, V.R. Troll (2012), A volcanotectonic survey of

814   Ascraeus Mons, Mars, *J. Geophys. Res., 117,* E01004, doi: 10.1029/2011JE003825.

815   Carr, M.H. (1973), Volcanism on Mars, *J. Geophys. Res.*, *78*, 4049 – 4062.

816   Carr, M.H. (1974), Tectonism and Volcanism of the Tharsis Region of Mars, *J. Geophys. Res.,*

817   *79, no. 26,* 3942 – 3949.

818   Cashman, K., Pinkerton, H., and J. Stephenson (1998), Introduction to special section: Long

819   lava flows, *J. Geophys. Res.*, 103, no. B11, 27,281–27,289.

820   Chemical Rubber Company (CRC) (1984), CRC Handbook of Chemistry and Physics. Weast,

821   Robert C., editor. 65th edition. *CRC Press, Inc*. Boca Raton, Florida. USA.

822   Christensen, P.R. (1986), Regional Dust Deposits on Mars: Physical Properties, Age, and

823   History, *J. Geophys. Res., 91, no. B3,* 3533 – 3545.

824   Christensen, P.R., B.M. Jakosky, H.H. Kieffer, M.C. Malin, H.Y. McSween, K. Nealson, G.L.

825   Mehall, S.H. Silverman, S. Ferry, M. Caplinger, and M. Ravine (2004), The Thermal

826   Emission Imaging System (THEMIS) for the Mars 2001 Odyssey Mission, *Space Sci. Rev.,*

827   *110,* 85 – 130.

828   Crane Company (1988), Flow of fluids through valves, fittings, and pipe, *Technical Paper No.*

829   *410* (TP 410).

830   Crown, D.A., and M.S. Ramsey (2016), Morphologic and thermophysical characteristics of lava

831   flows   southwest   of   Arsia   Mons,   Mars,   *J.   Volcanol.   Geotherm.   Res.*,

832   http://dx.doi.org/10.1016/j.volgeores.2016.07.008.

833   Crumpler, L.S., and J.C. Aubele (1978), Structural Evolution of Arsia Mons, Pavonis Mons, and

834   Ascraeus Mons: Tharsis Region of Mars, *Icarus*, 34, 496–511.

835   Dohm, J.M., Baker, V.R., Maruyama, S., and R.C. Anderson (2007), Traits and Evolution of the

836   Tharsis superplume, Mars, *Superplumes: Beyond Plate Tectonics*, 523 – 536.

837   Fink, J.H., Park, S.O., and R. Greeley (1983), Cooling and deformation of sulfur flows, *Icarus*,

838   56, 38–50.

839   Fink, J.H., and R. W. Griffiths (1990), Radial spreading of viscous-gravity currents with

840   solidifying crust, *J. Fluid Mech.*, 221, 485–509.

841   Garry, W.B., Zimbelman, J.R., and T.K.P. Gregg (2007), Morphology and emplacement of a

842   long-channeled lava flow near Ascraeus Mons volcano, Mars, *J. Geophys. Res.*, 112,

843   E08007, doi: 10.1029/2006JE002803.

844   Giacomini, L., Massironi, M., Martellato, E., Pasquare, G., Frigeri, A., and G. Cremonese

845   (2009), Inflated flows on Daedalia Planum (Mars)? Clues from a comparative analysis with

846   the Payen volcanic complex (Argentina), *Planet. Space Sci.,* 57, 556–570.

847   Giacomini, L., Carli, C., Sgavetti, M., and M. Massironi (2012), Spectral analysis and geological

848   mapping of the Daedalia Planum lava field (Mars) using OMEGA data, *Icarus*, 220, 679 –

849   693.

850   Glaze, L.S., and S.M. Baloga (2006), Rheologic inferences from the levees of lava flows on

851   Mars, *J. Geophys. Res.*, 111, E09006, doi: 10.1029/2005JE002585.

852   Glaze, L.S., Baloga, S.M., Garry, W.B., Fagents, S.A., and C. Parchetta (2009), A hybrid model

853   for leveed lava flows: Implications for eruption styles on Mars, *J. Geophys. Res.*, 114,

854   E07001, doi: 10.1029/2008JE003278.

855   Gorelick, N.S., Weiss-Malik, M., Steinber, B., and S. Anwar (2003), JMARS: A Multimission

856   Data Fusion Applciation, *34th Lunar and Planetary Science Conference*, abstract no. 2057.

Gregg, T.K.P., and J. H. Fink (1996), Quantification of extraterrestrial lava flow effusion rates through laboratory simulations, *J. Geophys. Res.*, 101, No. E7, pp. 16891–16900, 96JE01254.

Gregg, T.K.P., and J. H. Fink (2000), A laboratory investigation into the effects of slope on lava flow morphology, *J. Volcano. and Geotherm. Res.*, 96, 145–159.

Greeley, R., and P.D. Spudis (1981), Volcanism on Mars, *Rev. Geophys. Spac. Phys.*, 19, no. 1, 13 – 41.

Griffiths, R.W. and J.H. Fink (1992), The morphology of lava flows in planetary environments: predictions from analog experiments, *J. Geophys. Res. Solid Earth*, 97, B13, 19739–19748.

Guest, J.E., Kilburn, CRJ, Pinkerton, H., and A.M. Duncan (1987), The evolution of lava flow-fields: observations of the 1981 and 1983 eruptions of Mount Etna, Sicily, *Bull Volcanol*, 49, 527–540.

Harris, A.J.L., and S.K. Rowland (2015), Lava flows and rheology, *The Encyclopedia of Volcanoes 2nd Edition*, 321 – 342.

Hauber, E., Broz, P., Jagert, F., Jodlowski, P., and T. Platz (2011), Very recent and wide-spread basaltic volcanism on Mars, *Geophys. Res. Lett.*, 38, L10201, doi: 10.1029/2011GL047310.

Hiesinger, H., Head III, J.W., and G. Neukum (2007), Young lava flows on the eastern flank of Ascraeus Mons: Rheological properties derived from High Resolution Stereo Camera (HRSC) images and Mars Orbiter Laser Altimeter (MOLA) data, *J. Geophys. Res.*, 112, E05011, doi: 10.1029/2006JE002717.

Hon. K., Kauahikaua, J., Denliger, R., and K. Mackay (1994), Emplacmenet and inflation of pahoehoe sheet flows: observations and measurements of active lava flows of Kilauea volcano, Hawaii, *Geologic. Soc. Amer. Bull.*, 106, 351–370.

880 Hulme, G. (1974), The interpretation of lava flow morphology, *Geophys. J. R. astr. Soc.*, 39, 361

881   – 383.

882 Hulme, G. (1976), The Determination of the Rheological Properties and Effusion Rate of an

883   Olympus Mons Lava, *Icarus, 27,* 207 – 213.

884 Hulme, G., and G. Fielder (1977), Effusion rates and rheology of lunar lavas, *Phil. Trans. R. Soc.*

885   *Lond.* A., 285, 227 – 234.

886 Jaumann, R., G. Neukum, T. Behnke, T.C. Duxbury, K. Eichentopf, J. Flohrer., S. Van Gasselt,

887   B. Giese, K. Gwinner, E. Hauber, H. Hoffmann, A. Hoffmeister, U. Köhler, K.-D. Martz,

888   T.B. McCord, V. Mertens, J. Oberst, R. Pischel, D. Reiss, E. Ress, T. Roatsch, P. Saiger, F.

889   Scholten, G. Schwartz, K. Stephan, M. Wählisch and The HRSC Co-Investigator Team

890   (2007), The high-resolution stereo camera (HRSC) experiment on Mars Express: instrument

891   aspects and experiment conduct from interplanetary cruise through the nominal mission,

892   *Planet. Space Sci., 55,* 928 – 952.

893 Jeffreys, H. (1925), The flow of water in an inclined channel of rectangular section, *The London,*

894   *Ediburgh,   and   Dublin   Phil.   Mag.   J.   Sci.*,   49:293,   793   –   807,   doi:

895   10.1080/14786442508634662.

896 Lipman, P.W., and N.G. Banks (1987), AA Flow dynamics, Mauna Loa, *Volcanism in Hawai'i*,

897   1527 – 1567.

898 Malin, M.C., J.F. Bell, B.A. Cantor, M.A. Caplinger, W.M. Calvin, R.T. Clancy, K.S. Edgett, L.

899   Edwards, R.M. Haberle, P.B. James, S.W. Lee, M.A. Ravine, P.C. Thomas, and M.J. Wolff

900   (2007), Context camera investigation on board the Mars Reconnaissance Orbiter, *J. Geophys.*

901   *Res., 112*, E05S04, doi: 10.1029/2006JE002808.

902   McEwan, A.S., E.M. Eliason, J.W. Bergstrom, N.T. Bridges, C.J. Hansen, W.A. Delamere, J.A.

903   Grant, V.C. Gulick, K.E. Herkenhoff, L. Keszthelyi, R.L. Kirk, M.T. Mellon, S.W. Squyres,

904   N. Thomas, and C.M. Weitz (2007), Mars Reconnaissance Orbiter's High-Resolution

905   Imaging Science Experiment (HiRISE), *J. Geophys. Res., 112,* E05S02,

906   doi:10.1029/2005JE002605.

907   Mellon, M.T., Jakosky, B.M., Kieffer, H.H., and P.R. Christensen (2000), High-resolution

908   thermal inertia mapping from the Mars Global Surveyor Thermal Emission Spectrometer,

909   *Icarus*, 148, 437 – 455, doi: 10.1006/icar.2000.6503.

910   Moore, H.J., Arthur, D.W.G., Schaber, G.G. (1978), Yield strengths of flows on the Earth, Mars,

911   and Moon, *Proc. Lunar Planet. Sci. Conf. 9th*, 3351 – 3378.

912   Nichols, R. L. (1939), Viscosity of Lava, *J. Geology*, 47, no. 3, 290 – 302.

913   Neukum, G., R. Jaumann., H. Hoffmann, H., E. Hauber, J.W. Head, A.T. Basilevsky, B.A.

914   Ivanov, S.C. Werner, S. van Gasselt, J.B. Murray, T. McCord, and The HRSC Co-

915   Investigator Team (2004), Recent and episodic volcanic and glacial activity on Mars revealed

916   by the High-Resolution Stereo Camera, *Nature*, 432, 971 – 979.

917   Pasckert, J. H., Hiesinger, H., and D. Reiss (2012), Rheologies and ages of lava flows on

918   Elysium Mons, Mars, *Icarus*, 219, 443 – 457.

919   Peck, D.L. (1978), Cooling and Vesiculation of Alae Lava Lake, Hawai'i, *Geologic. Surv. Pro.*

920   *Paper*, 935-B.

921   Peters, S.I. (2020), Investigating Lava Flow Emplacement: Implications for Volcanic Hazards

922   and Planetary Evolution, *Arizona State University*, *ProQuest Dissertations Publishing*,

923   thesis.

924   Peters, S.I., and P.R. Christensen (2017), Flank vents and graben as indicators of Late

925   Amazonian volcanotectonic activity on Olympus Mons, *J. Geophys. Res. Planets*, 112,

926   doi:10.1002/2016JE005108.

927   Peiterson, M.N., and D.A. Crown (1999), Downflow width behavior of Martian and terrestrial

928   lava flows, *J. Geophys. Res.*, 104, no. E4, 8473 – 8488.

929   Pieri, D.C., Baloga, S.M., Nelson, R.M., and C. Sagan (1984), Sulfur Flows of Ra Patera, IO,

930   *Icarus*, 60, 685 – 700.

931   Pinkerton, H. (1987), Factors affecting the morphology of lava flows, *Endeavour New Series*, 11,

932   no. 2, 73–79.

933   Pinkerton, H., and R.S. J. Sparks (1976), The 1975 Sub-terminal lavas, Mount Etna: A case

934   history of the formation of a compound lava field, *J. Volcanol. Geotherm. Res.*, 1, 167 – 182.

935   Pinkerton, H., James, M., and A. Jones (2002), Surface measurements of active lava flows on

936   Kilauea volcano, Hawai'i, *J. Volcanol. Geotherm. Res.*, 113, 159 – 176.

937   Plescia, J.B. (2004), Morphometric properties of Martian volcanoes, *J. Geophys. Res., 109,*

938   E03003, doi: 10.1029/2002JE002031.

939   Rogers, A.D., and P.R. Christensen (2007), Surface mineralogy of Martian low-albedo regions

940   from MGS-TES data: implications for upper crustal evolution and surface alteration, *J.*

941   *Geophys. Res.*, 112, E01003, doi: 10.1029/2006JE002727.

942   Rowland, S.K., Harris, A.J.L., and H. Garbeil (2004), Effects of Martian conditions on

943   numerically modeled, cooling-limited, channelized lava flows, *J. Geophys. Res.*, 109,

944   E10010, doi: 10.1029/2004JE002288.

945   Sakimoto, S.E.H., Crips, J., and S.M. Baloga (1997), Eruption constraints on tube-fed planetary

946   lava flows, *J. Geophys. Res.*, 102, no. E3, 6597 – 6613.

947   Sakimoto, S.E.H., and T.K.P. Gregg (2001), Channeled flow: analytic solutions, laboratory

948   experiments, and applications to lava flows, *J. Geophys. Res.*, 106, no. B5, 8629–8644.

949   Scott, D.H., and K. L. Tanaka (1981), Mars: Paleostratigraphic restoration of buried surfaces in

950   Tharsis Montes, *Icarus*, 45, 304 – 319.

951   Self, S., Thordarson T., Kesthelyi, L., Walker, G.P.L., Hon, K., Murphy, M.T., Long, P., and S.

952   Finnemore (1996), A new model for the emplacement of Colombia River basalts as large,

953   inflated pahoehoe lava flow fields, *Geophys. Res. Lett.*, 23, no. 19, 2689–2692.

954   Self, S., Thordarson, T., and L. Keszthelyi (1997), Emplacement of Continental Flood Basalt

955   Lava Flows, *Geophys. Monograph.*, 100, 381 – 410.

956   Self, S., Jay, A.E., Widdowson, M., and L.P. Keszthelyi (2008), Correlation of the Deccan and

957   Rajahmundry Trap lavas: Are these the longest and largest lava flows on Earth?, *J. Volcanol.*

958   *Geotherm. Res.*, 172, 3 – 19.

959   Sheth, H.C., 2006. The emplacement of pahoehoe lavas on Kilauea and in the Deccan Traps. *J.*

960   *Earth Systems Sci.,* 115, 615–629.Soule, S.A., and K.V. Cashman (2004), The mechanical

961   properties of solidified polyethylene glycol 600, an analog for lava crust, *J. Volcanol.*

962   *Geotherm. Res.*, 129, 139–153.

963   Spudis, P.D., McGovern, P.J., and W.S. Kiefer (2013), Large shield volcanoes on the Moon, *J.*

964   *Geophys. Res. Planets*, 118, 1063 – 1081, doi: 10.1002/jgre.20059.

965   Vicari, A., Alexis, H., Del Negro, C., Coltelli, M., Marsella, M., and C. Proietti (2007),

966   Modelling of the 2001 lava flow at Etna volcano by cellular automata approach,

967   *Environment. Model. Software*, 22, 1465–1471.

968   Wadge, G. (1981), The variation of magma discharge during basaltic eruptions, *J. Volcanol.*

969   *Geotherm. Res.*, 11, 139–168.

970   Walker, G.P.L. (1971), Compound and simple lava flows and flood basalts, *Bull. Volcanol.*, 35,
971   579 – 590.

972   Walker, G.P.L. (1973), Lengths of lava flows, *Phil. Trans. R. Soc. Lond. A.*, 274, 107 – 118.

973   Werner, S.C. (2009), The global martian volcanic evolutionary history, *Icarus*, 201, 44 – 68.

974   Wilson, L., J.W. Head III (1983) A comparison of volcanic eruption processes on Earth, Moon,
975   Mars, Io, and Venus, *Nature*, 302, 663 – 669.

976   Wolfe, E.W., Garcia, M.O., Jackson, D.B., Koyanagi, R.Y., Neal, C.A., and A.T. Okamura
977   (1987), The Pu'u O'o eruption of Kilauea volcano, episodes 1 – 20, January 3, 1983, to June
978   8, 1984, 471 – 508.

979   Xiao, L., Huang, J., Christensen, P.R., Greeley, R., Williams, D.A., Zhao J., and Q. He (2012),
980   Ancient volcanism and its implication for thermal evolution of Mars, *Earth and Planet. Sci.*
981   *Lett.*, 323-324, 9 – 18.

982   Zuber, M.T., D.E. Smith, S.C. Solomon, D.O. Muhleman, J.W. Head, J.B. Garvin, J.B. Abshire,
983   and J.L. Bufton (1992), The Mars observer laser altimeter investigation, *J. Geophys. Res., 97,*
984   7781 – 7797.